

Electronic Supplementary Information (ESI) for *Journal of Materials Chemistry A*

# Enhanced efficiency and stability of PTB7-Th-based multi-non-fullerene solar cells enabled by the working mechanism of the coexisting alloy-like structure and energy transfer model

Sora Oh,<sup>†ab</sup> Chang Eun Song,<sup>†bc</sup> Taeho Lee,<sup>†d</sup> Ara Cho,<sup>a</sup> Hang Ken Lee,<sup>c</sup> Jong-Cheol Lee,<sup>ab</sup> Sang-Jin Moon,<sup>bc</sup> Eunhee Lim,<sup>\*d</sup> Sang Kyu Lee,<sup>\*ab</sup> Won Suk Shin<sup>\*bce</sup>

<sup>a</sup>Advanced Materials Division, Korea Research Institute of Chemical Technology (KRICT), 141 Gajeongro, Yuseong, Daejeon 34114, Republic of Korea. E-mail: skyulee@kRICT.re.kr

<sup>b</sup>Advanced Materials and Chemical Engineering, University of Science and Technology (UST), 217 Gajeongro, Yuseong, Daejeon 34113, Republic of Korea.

<sup>c</sup>Energy Materials Research Center, Korea Research Institute of Chemical Technology (KRICT), 141 Gajeongro, Yuseong, Daejeon 34114, Republic of Korea. E-mail: shinws@kRICT.re.kr

<sup>d</sup>Department of Chemistry, Kyonggi University, 154-42 Gwanggyosan-ro, Yeongtong-gu, Suwon 16227, Republic of Korea. E-mail: ehlim@kyonggi.ac.kr

<sup>e</sup>KU-KRICT Collaborative Research Center & Division of Display and Semiconductor Physics & Department of Advanced Materials Chemistry, Korea University, 2511 Sejong-ro, Sejong 30019, Republic of Korea.

<sup>†</sup>First authors

S.O., C.E.S. and T.L. contributed equally to this work.

\*Corresponding Author

E.L.: ehlim@kyonggi.ac.kr, S.K.L.: skyulee@kRICT.re.kr, W.S.S.: shinws@kRICT.re.kr

## Experimental section

### *Materials*

All chemicals and solvents were purchased from Aldrich and were used without further purification. The T2-ORH non-fullerene acceptor was synthesized as follow reference.<sup>1</sup> The materials of PTB7-Th, EH-IDTBR and ITIC were purchased from one-materials. And the PC<sub>71</sub>BM fullerene acceptor was purchased from OSM (Republic of Korea).

### *DSC analysis*

DSC experiments were carried out with a Mettler Toledo DSC822 instrument at a heating rate of 10 °Cmin<sup>-1</sup> under nitrogen. Pure EH-IDTBR and T2-ORH were used directly and the sample of 1:1 blended T2-ORH:EH-IDTBR was prepared by drop-casting the materials from CHCl<sub>3</sub> solution directly into the DSC pan and allowing the solvent to evaporate under Ar.

### *PL spectroscopy*

Thin films were excited at 500, 650 nm with a solid state laser in continuous wave operation (MGL-III-532, Changchun New Industries) at an excitation power of 80 mW. The laser beam was expanded to a spot size of 6 mm in diameter in order to probe a rather large sample volume. Photoluminescence was fiber-coupled into a spectrograph (Acton Research SpectraPro 300i) and detected with an intensified CCD (Princeton Research, PiMax 512).

### *CV measurement*

CV was carried out using an IviumStat instrument under argon using 0.1 M tetrabutylammonium tetrafluoroborate (TBABF<sub>4</sub>) solution in acetonitrile at a scan rate of 50 mVs<sup>-1</sup> at 25 °C. A Pt wire, Ag/AgCl electrode, and a platinum electrode coated with polymer film were used as the counter, reference, and working electrodes, respectively. The HOMO and LUMO energy level was determined by measuring the oxidation onsets ( $E_{ox}$ ) and reduction onsets ( $E_{red}$ ) of the products. The HOMO and LUMO were calculated using this equation:  $E_{HOMO} = -(E_{onset,ox} - E_{1/2,ferrocene} + 4.8)$  eV and  $E_{LUMO} = -(E_{onset,red} - E_{1/2,ferrocene} + 4.8)$  eV.

### *Fabrication of the ternary-blend organic solar cells (OSCs)*

In this study, the ternary-blend OSCs were fabricated with the structure ITO/ZnO NPs/PEIE/photoactive layer/MoO<sub>x</sub>/Ag. The procedure for cleaning the patterned ITO glass substrates included sonication and rinsing in deionized water with the detergent, acetone, and isopropyl alcohol. All the cleaned ITO substrates were treated with UV ozone for 15 min. A thin layer of ZnO NPs (30 nm) was spin coated onto the ITO and then annealed at 100 °C for 10 min in air. The polyethylenimine, 80% ethoxylated (PEIE) solution was prepared by dissolving PEIE in ethanol at a weight concentration of 0.1 wt%. The PEIE layer (5 nm) was deposited onto the ZnO films at 4000 rpm for 60 s and then annealed immediately at 100 °C, for 10 min. After that, ITO/ZnO NPs/PEIE substrates were transferred to the nitrogen-filled glovebox for deposition of the photoactive layer. The donor:acceptor (1.0:2.0, w/w) solutions dissolved in chloroform were spin-cast on top of the PEIE layer. Then the photoactive layers were placed in a glass petri dish containing 150 μL CHCl<sub>3</sub> (CF) for solvent vapor annealing (SVA) for 15 s. Finally, 10 nm thick MoO<sub>x</sub> and 100 nm Ag were deposited successively to complete the inverted OSCs.

### *Fabrication of tandem OSCs*

ITO/ZnO NPs/PEIE substrates were prepared via the same process as ternary-blend OSCs. After that, the PTB7-Th:T2-ORH (1.0:2.0, w/w) solutions was spin coated on the ITO/ZnO NPs/PEIE substrate to form a photoactive layer for a bottom cell. The modified PEDOT:PSS solution was spin coated on top of the PTB7-Th:T2-ORH at a spin rate of 4000 rpm for 60s and annealed at 100 °C, for 10 min to remove residuary water in the PEDOT:PSS layer. After that, ZnO NPs solution was spin coated on top of the PEDOT:PSS layer. Then PEIE solution was spin-coated onto the ZnO NPs layer and the PEIE coated device was baked at 100 °C, for 10 min on the hot plate. The PTB7-Th:EH-IDTBR photoactive layer for the top cell was spin coated onto PEIE coated device. All of the photoactive layers were annealed by SVA with CF for 15 s. The tandem OSCs were completed after deposition of 10 nm MoO<sub>x</sub> and 100 nm Ag as the anode.

### *Fabrication of sub-module OSCs*

The stripe patterned ITO glass substrate (5cm x5cm) was washed deionized water with the detergent, acetone and isopropyl alcohol using ultra-sonicator and dried in oven at 120 °C for 4 hours. Sub-module OSCs were fabricated with total 6 stripe cells. Before the fabrication, ITO glass was then treated with UV-ozone for 30min; ZnO NPs layer (30nm) was coated on the ITO substrate by using spin-casting. Then it was dried at 100 °C for 10min in air. And then PEIE layer as the interfacial modifier between ZnO and photoactive layer was coated on the ITO/ZnO NPs substrate at 4000 rpm for 60 s. A solution of PTB7-Th:T2-ORH:EH-IDTBR (1:1:1) materials dissolved in CF deposited on the ZnO NPs/PEIE layer. Finally, the MoO<sub>x</sub>/Ag (10/100nm) top electrode was deposited by thermal evaporator after the tape-masking for insulation of each stripe cell.

### *OSCs characterization*

The current-voltage characteristics of OSCs were measured under simulated 100 mW/cm<sup>2</sup> AM 1.5G irradiation from a Xe arc lamp with an AM 1.5 global filter. The light source was calibrated by using an NREL-certified silicon reference cell with an integrated KG1 optical filter. The EQE was measured by underfilling the device area using a reflective microscope objective to focus the light output from a 100 W Xe arc lamp outfitted with a monochromator and optical chopper; the photocurrent was measured using a lock-in amplifier, and the absolute photon flux was determined using a calibrated silicon photodiode. The study of light intensity dependence was done using a set of neutral density filters (Newport), allowing a range of intensity from 3.2 to 100 mW cm<sup>-2</sup>. All device measurements were carried out in air at room temperature.

### *GIWAXS characterization*

2D-GIWAX measurements were performed on the PLS-II 3C beam line at the Pohang Accelerator Laboratory in Republic of Korea. The photoactive layers were coated on Si/ZnO NPs/PEIE substrate with optimized device fabrication conditions. The monochromatic X-ray beam with intensity 10.0833 keV was adjusted with incident angle 0.11-0.14° on sample, which maximized on the scattering intensity from the bulk photoactive films. The scattered X-ray patterns were recorded with charge coupled device (CCD) detector.

### *Hole and electron mobility measurements*

The hole and electron mobility of donor:acceptor blend films were measured by using SCLC method. The hole-only (ITO/PEDOT:PSS/donor:acceptor/Au) and electron-only (ITO/ZnO NPs/PEIE/donor:acceptor/Ca/Al) devices were fabricated and all photoactive layers annealed with SVA by CF for 15s. The charge carrier mobility were determined by fitting dark  $J$ - $V$  curves in the 0-3 V range into space charge limited form and mobility ( $\mu$ ) calculated using equation  $J = 9\epsilon_0\epsilon_r\mu V^2/8L^3$ , where  $J$  = current density,  $\epsilon_r$  = dielectric constant of the transport medium,  $\epsilon_0$  = permittivity of free space ( $8.85 \times 10^{-12}$  F m<sup>-1</sup>),  $V$  = internal voltage and  $L$  = thickness of photoactive layers, respectively.

#### *IMPS and IMVS analysis*

Intensity modulated photocurrent and photovoltage spectroscopy (IMPS/IMVS) methods were performed using an IviumStat instrument (Ivium Technologies) equipped with a four-wire impedance test interface (in a two-probe configuration). Both the DC and AC components of the illumination were provided by a red-emitting LED ( $\lambda = 635$  nm,  $V_{\text{appl}} = 1.5$  V) as the light source for this study. IMPS and IMVS were measured over the range of  $5 \times 10^5$  Hz to  $8 \times 10^5$  Hz under short-circuit and over the range of  $3 \times 10^3$  Hz to  $1 \times 10^5$  Hz under open-circuit conditions, respectively.

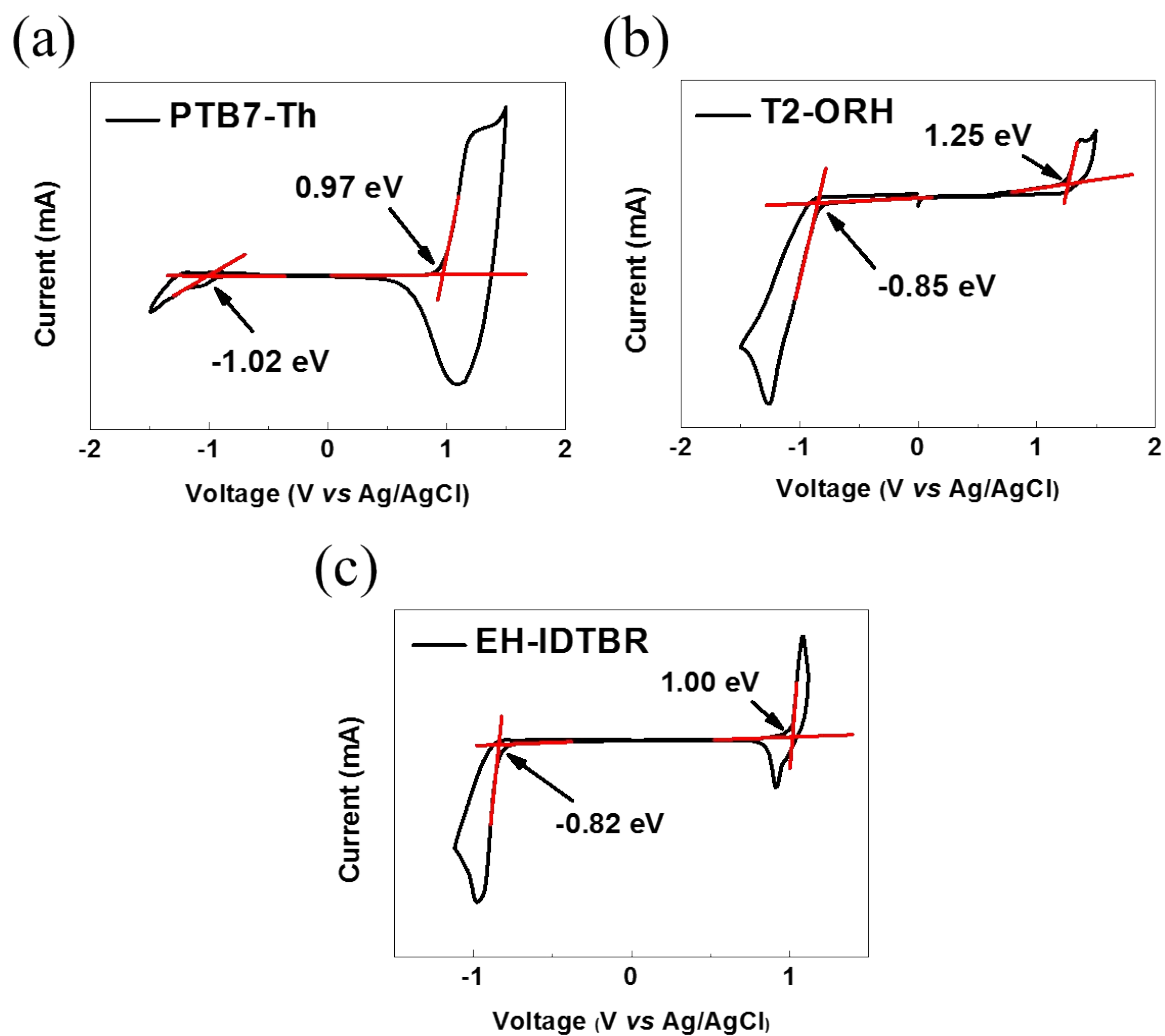
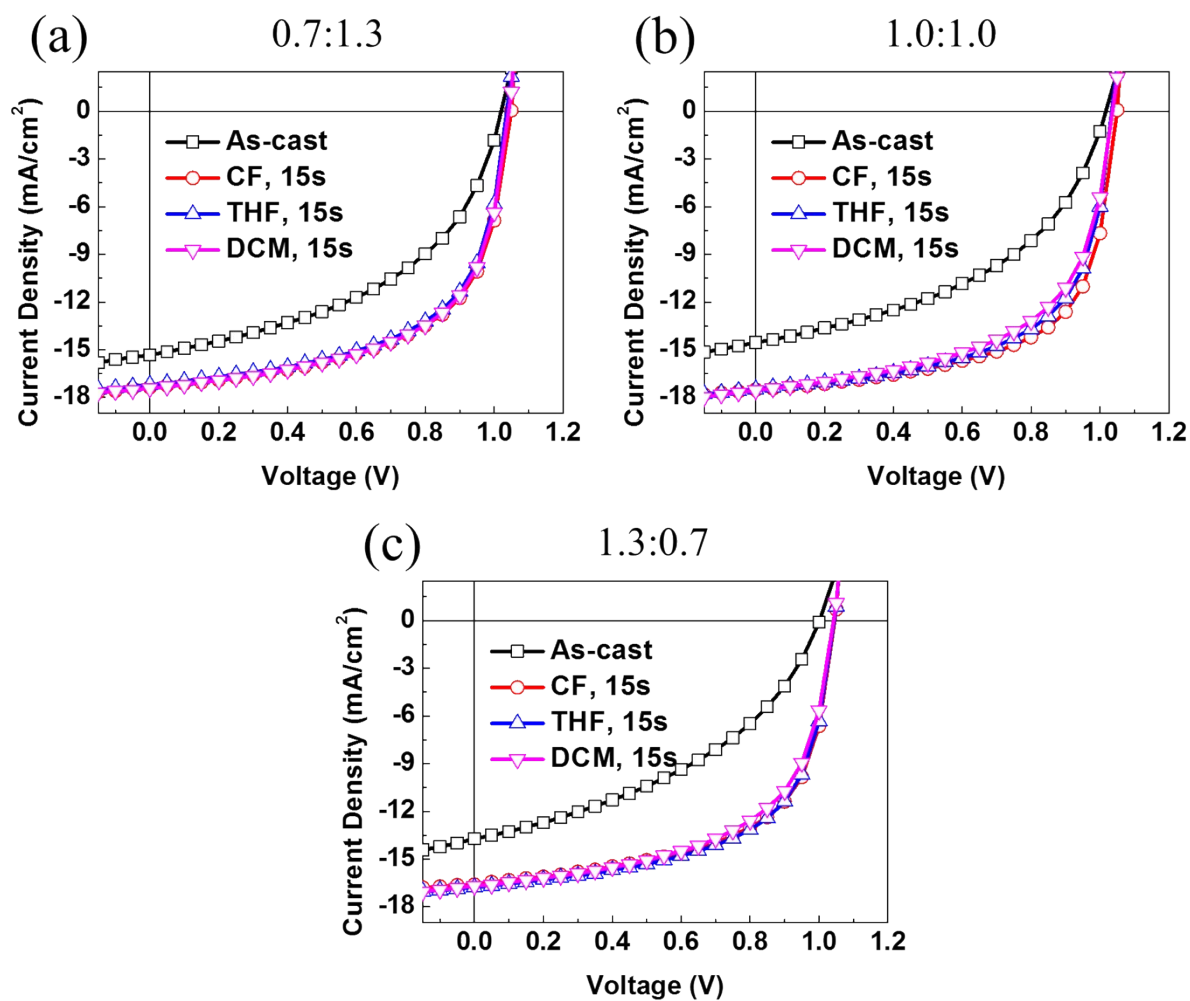


Fig. S1 Cyclic voltammetry (CV) of (a) PTH7-Th, (b) T2-ORH, (c) EH-IDTBR.

**Table S1** Photovoltaic properties of ternary-blend OSCs with different T2-ORH:EH-IDTBR blend ratio and solvent vapor annealing systems under AM 1.5G illumination<sup>a</sup>

Acceptor	SVA	V <sub>oc</sub> [V]	J <sub>sc</sub> [mA/cm <sup>2</sup> ]	FF [%]	PCE [%]
T2-ORH:EH-IDTBR = 0.7:1.3	As-cast	1.02	15.33	47	7.39
	CF, 15s	1.05	17.36	60	10.87
	THF, 15s	1.04	17.20	59	10.59
	DCM, 15s	1.04	17.43	59	10.78
T2-ORH:EH-IDTBR = 1.0:1.0	As-cast	1.02	14.55	46	6.80
	CF, 15s	1.05	17.51	63	11.55
	THF, 15s	1.03	17.48	61	10.96
	DCM, 15s	1.04	17.56	58	10.56
T2-ORH:EH-IDTBR = 1.3:0.7	As-cast	1.00	13.73	41	5.70
	CF, 15s	1.05	16.61	61	10.52
	THF, 15s	1.04	16.79	60	10.57
	DCM, 15s	1.04	16.68	58	10.07

<sup>a</sup>Inverted device architecture is ITO/ZnO NPs/PEIE/photoactive layer( $d = \sim 100\text{nm}$ )/MoO<sub>x</sub>/Ag.

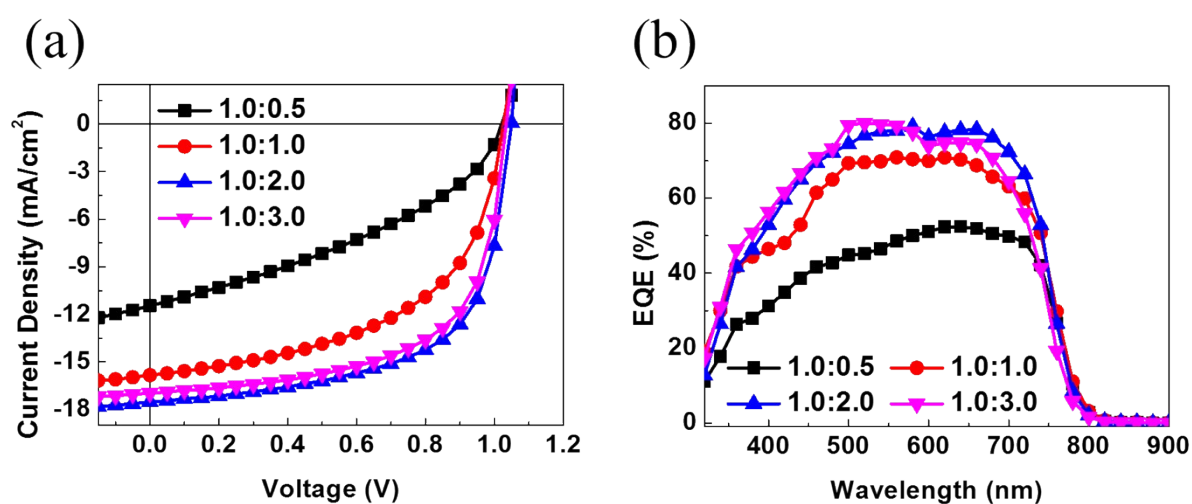


**Fig. S2**  $J$ - $V$  curves of ternary-blend OSCs with various solvent vapor annealing systems and T2-ORH:EH-IDTBR blend ratio for (a) 0.7:1.3, (b) 1.0:1.0, (c) 1.3:0.7.

**Table S2** Photovoltaic properties of donor:acceptor with different blend ratio under AM 1.5G illumination<sup>a</sup>

donor:acceptor [w/w]	$V_{oc}$ [V]	$J_{sc}$ [mA/cm <sup>2</sup> ]	$FF$ [%]	PCE [%]
1.0:0.5	1.02	11.46	38	4.43
1.0:1.0	1.03	15.83	54	8.72
1.0:2.0	1.05	17.51	63	11.55
1.0:3.0	1.03	16.96	62	10.92

<sup>a</sup>The devices architecture is ITO/ZnO NPs/PEIE/photoactive layer/MoO<sub>x</sub>/Ag and all photoactive layers are annealed by SVA using CF for 15s.

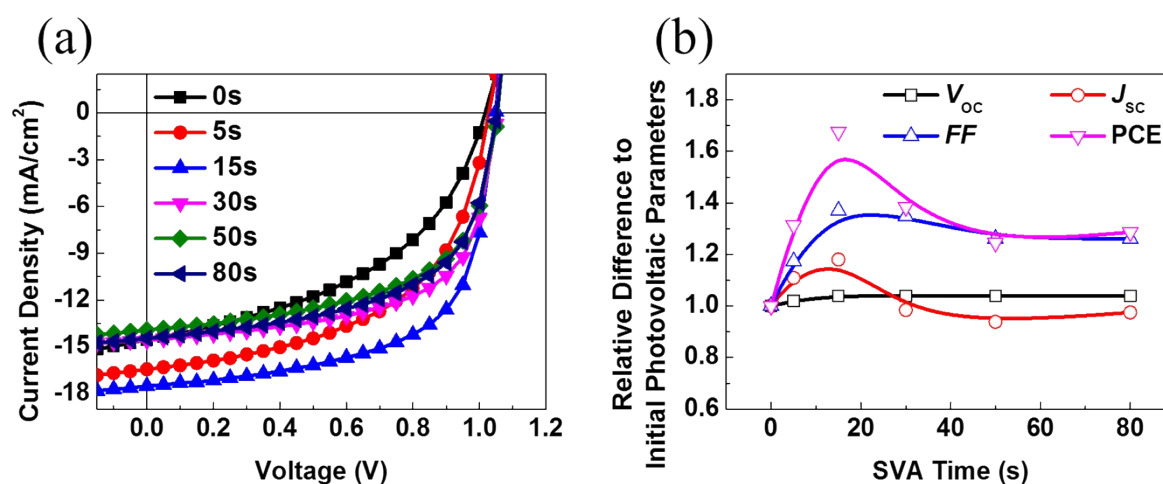
**Fig. S3.** (a)  $J$ - $V$  and (b) EQE curves of ternary-blend OSCs with different donor:acceptor blend ratio.

**Table S3** Photovoltaic properties of PTB7-Th:T2-OEH:EH-IDTBR (1:1:1) with different  $\text{CHCl}_3$  vapor annealing time under AM 1.5G illumination<sup>a</sup>

SVA Time <sup>b</sup> [s]	$V_{\text{oc}}$ [V]	$J_{\text{sc}}$ [mA/cm <sup>2</sup> ]	$FF$ [%]	PCE [%]
0	1.01	14.83	46	6.89
5	1.03	16.44	54	9.05
15	1.05	17.51	63	11.55
30	1.05	14.60	62	9.54
50	1.05	13.92	58	8.58
80	1.05	14.46	58	8.86

<sup>a</sup>The devices architecture is ITO/ZnO NPs/PEIE/photoactive layer( $d = \sim 100\text{nm}$ )/ $\text{MoO}_x/\text{Ag}$ .

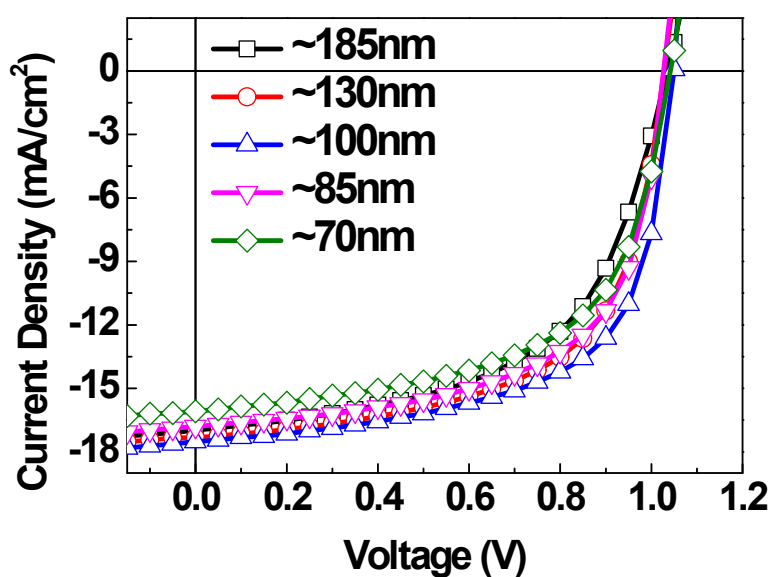
<sup>b</sup>All photoactive layers are annealed by SVA using CF.

**Fig. S4** (a)  $J$ - $V$  curves and (b) relative difference to initial photovoltaic parameters as a function of SVA time.

**Table S4** Photovoltaic properties of PTB7-Th:T2-OEH:EH-IDTBR (1:1:1) with different photoactive layer thickness under AM 1.5G illumination<sup>a</sup>

Thickness [nm]	$V_{oc}$ [V]	$J_{sc}$ [mA/cm <sup>2</sup> ]	$FF$ [%]	PCE [%]
~185	1.03	16.98	56	9.85
~130	1.03	17.33	61	10.82
~100	1.05	17.51	63	11.55
~85	1.03	16.80	62	10.62
~70	1.04	16.08	59	9.91

<sup>a</sup>The devices architecture is ITO/ZnO NPs/PEIE/photoactive layer/MoO<sub>x</sub>/Ag and all photoactive layers are annealed by SVA using CF for 15s.

**Fig. S5** *J-V* curves with different photoactive layer thickness in ternary-blend OSCs.

Device ID : OPV #1  
Date of Test : December 29, 2016  
Simulator : WACOM, WXS-155S-L2 (Class-AAA)  
Reference solar cell : KIER-PS-FD #1  
Test condition : STC (AM1.5G, 100 mW/cm<sup>2</sup>, 25.0 ± 1.0 °C)

Device Area : 0.04 cm<sup>2</sup> (차광 마스크 적용 면적)  
Sample Type : Organic solar cell (glass plate based)

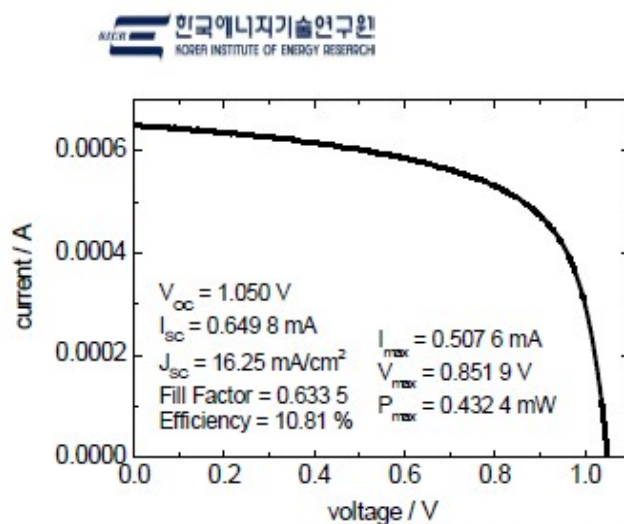


**Fig. S6** *I*-*V* curve and photovoltaic parameters of the optimum ternary-blend OSC certified by the Korea Institute of Energy Research (KIER).

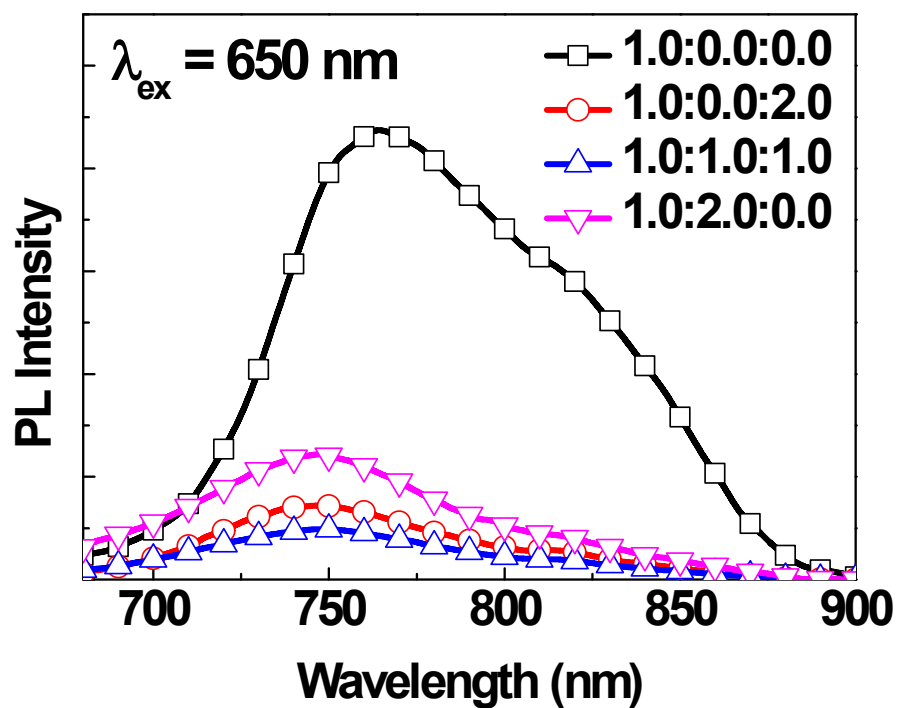


**Fig. S7** The PL spectrum of PTB7-Th film and PTB7-Th:T2-ORH:EH-IDTBR blend films with different ratios of PTB7-Th excited at 650 nm.

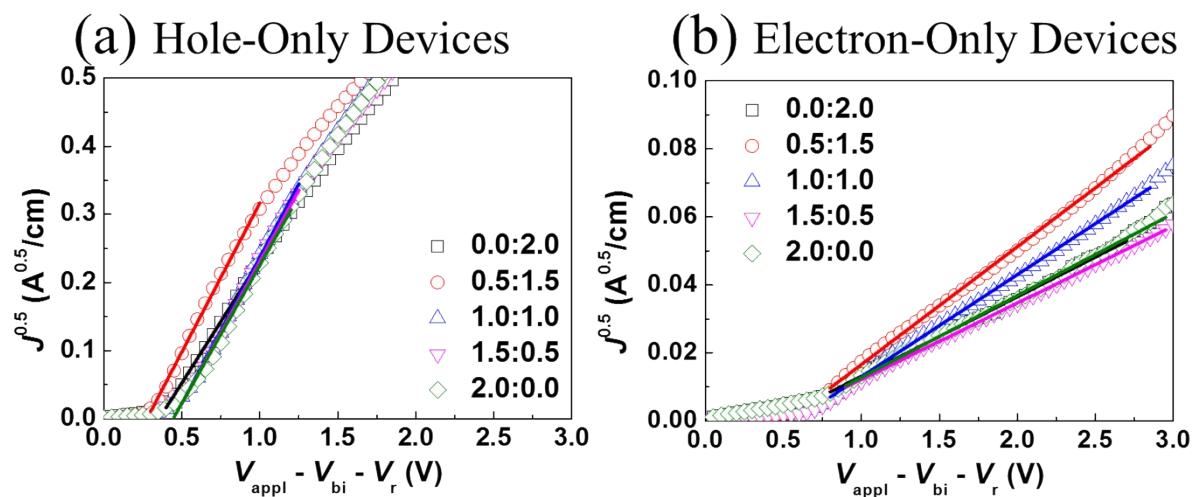
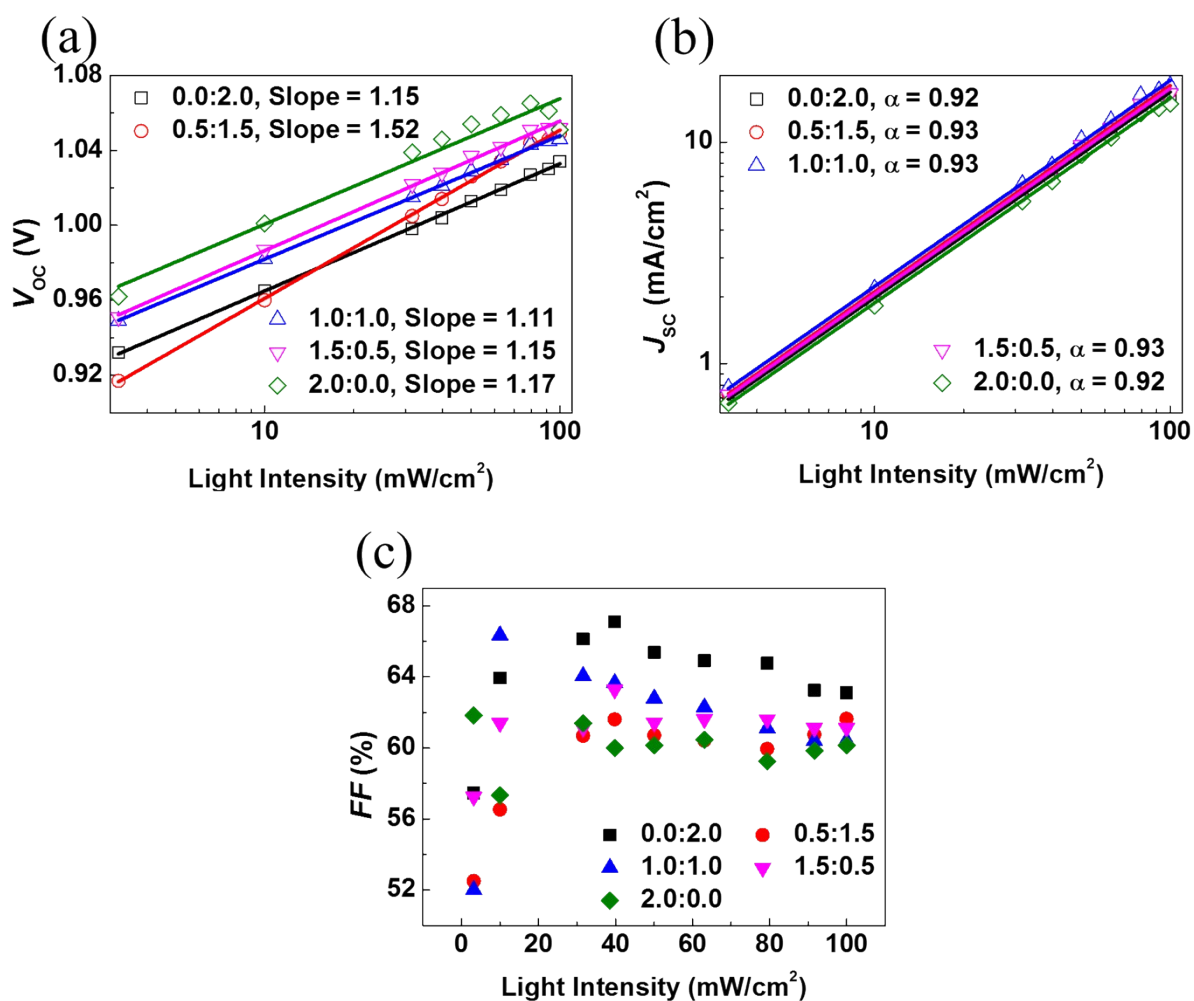
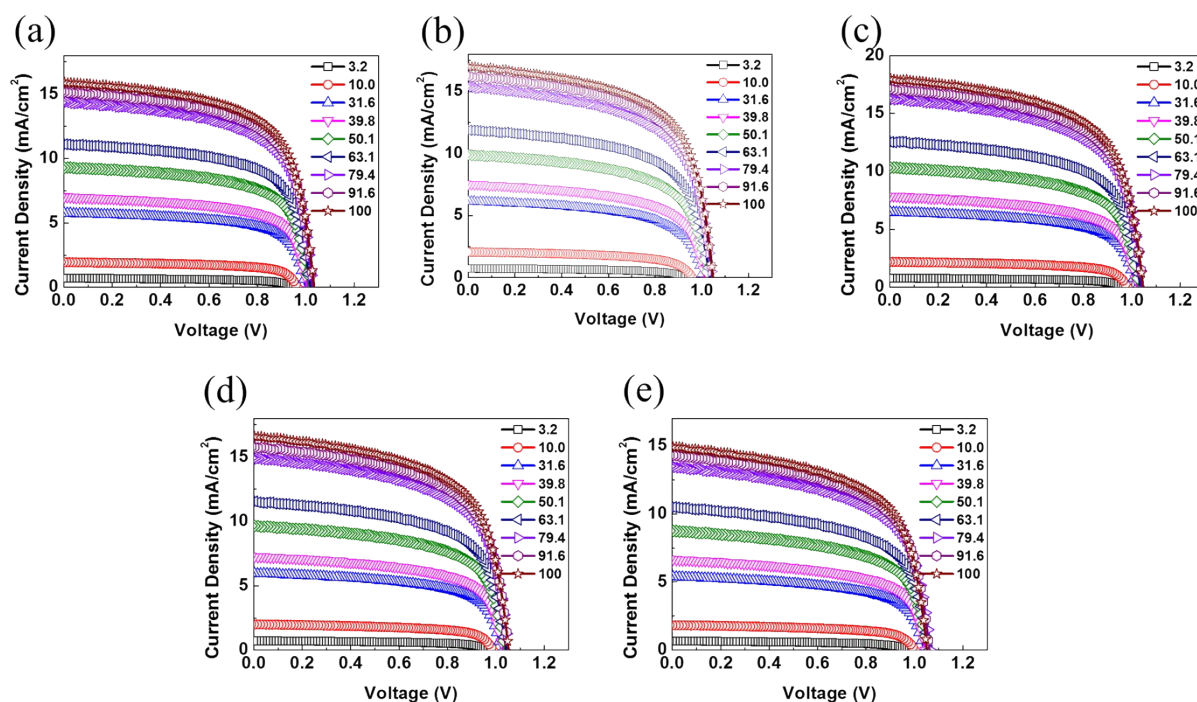


Fig. S8 Dark  $J$ - $V$  characteristics from (a) the hole-only and (b) electron-only devices.



**Fig. S9** Measured (a)  $V_{OC}$ , (b)  $J_{SC}$  and (c)  $FF$  of the ternary-blend OSCs with different blend ratio against light intensity.



**Fig. S10** Light intensity-dependent  $J$ - $V$  curves in ternary-blend OSCs for the (a) 0.0:2.0 (T2-ORH:EH-IDTBR), (b) 0.5:1.5 (T2-ORH:EH-IDTBR), (c) 1.0:1.0 (T2-ORH:EH-IDTBR), (d) 1.5:0.5 (T2-ORH:EH-IDTBR), (e) 2.0:0.0 (T2-ORH:EH-IDTBR) blend ratio.

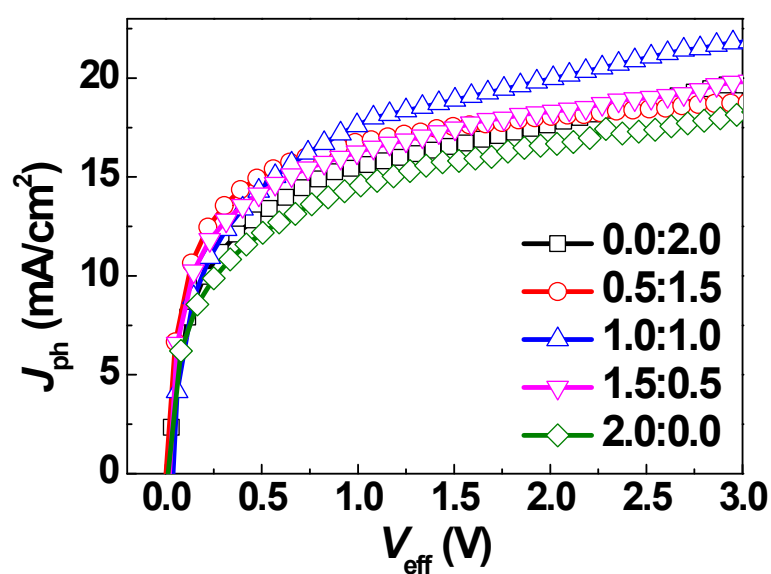


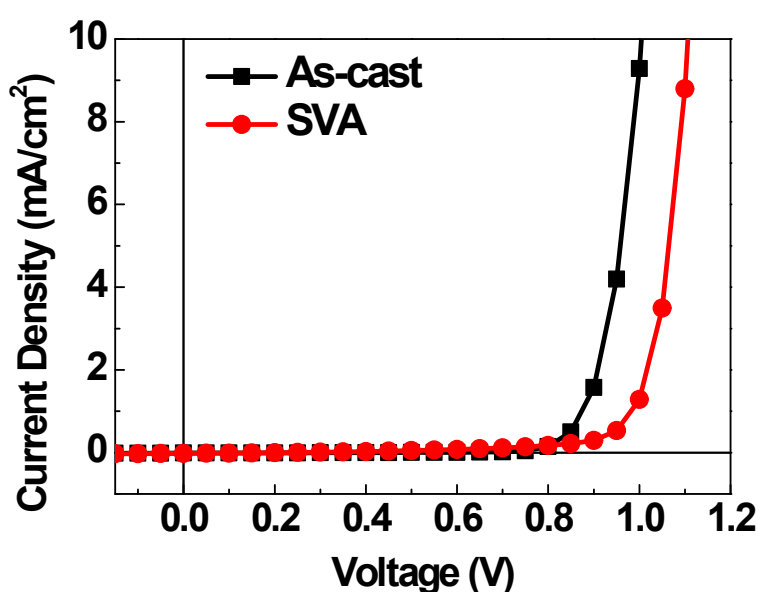
**Fig. S11** Photocurrent density dependence on the effective voltage of ternary-blend OSCs.

**Table S5** Photovoltaic properties of T2-OEH:EH-IDTBR (1:1) devices with as-cast and solvent vapor annealing under AM 1.5G illumination<sup>a</sup>

Annealing	$V_{oc}$ [V]	$J_{sc}$ [mA/cm <sup>2</sup> ]	$FF$ [%]	PCE [%]
As-cast	0.46	0.01	28	0.00
SVA <sup>b</sup>	0.23	0.02	28	0.00

<sup>a</sup>The devices architecture is ITO/ZnO NPs/PEIE/photoactive layer( $d \approx 100\text{nm}$ )/MoO<sub>x</sub>/Ag.

<sup>b</sup>The photoactive layers are annealed by solvent vapor annealing (SVA) using CF, for 15s.

**Fig. S12**  $J$ - $V$  curves for the devices based on T2-ORH:EH-IDTBR (1.0:1.0) photoactive layer with as-cast (black) and SVA (red) under AM 1.5G illumination with a light intensity of  $100 \text{ mW cm}^{-2}$ .

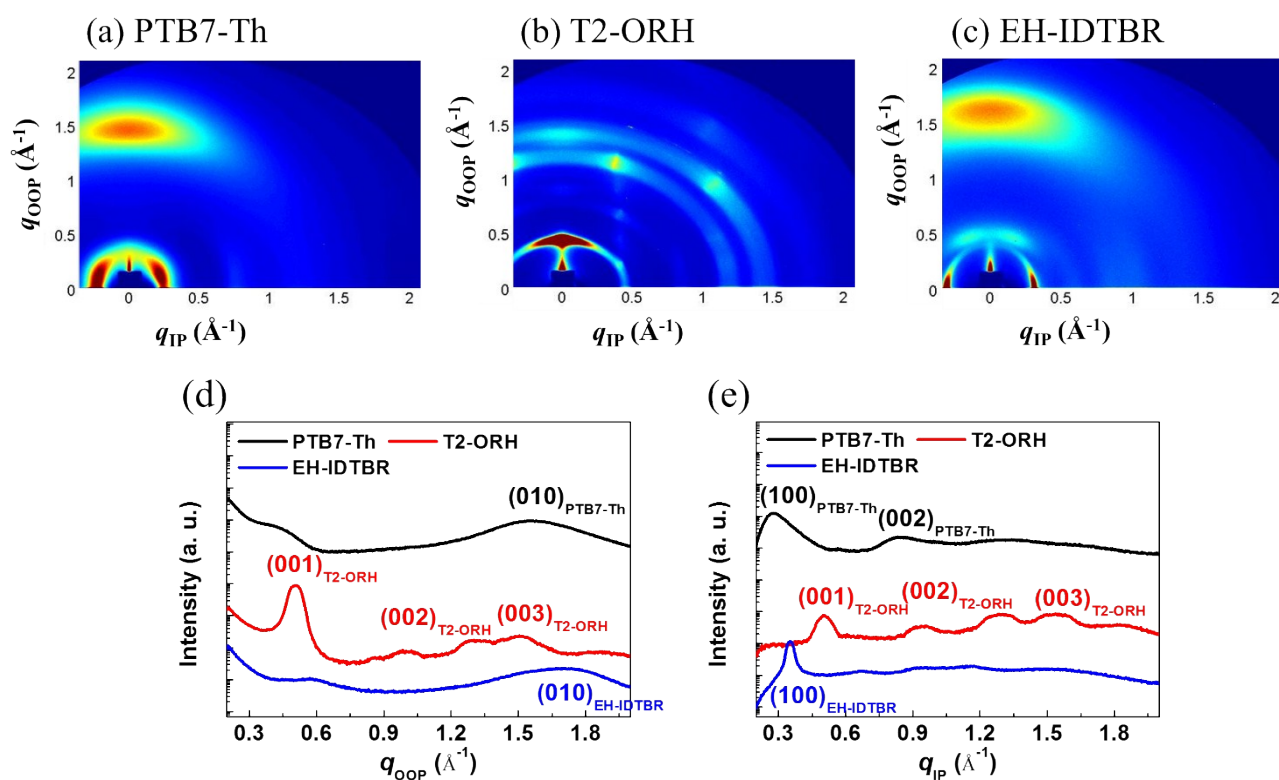


**Fig. S13** 2D GIWAXS patterns of (a) PTB7-Th, (b) T2-ORH and (c) EH-IDTBR. One-dimensional integrated scattering profiles for the corresponding films in the (f) out-of plane, (g) in-plane direction.

**Table S6** Packing parameters of SVA treated pure components derived from GIWAXS measurements

Film <sup>c</sup>	(100) <sup>a</sup> [Å]	(001) <sup>a</sup> [Å]	(010) <sup>a</sup> [Å]	(100) <sup>b</sup> [Å]	(002) <sup>b</sup> [Å]	(010) <sup>b</sup> [Å]
PTB7-Th	-	-	3.93	23.93	7.33	-
T2-ORH	-	12.44	-	-	6.59	-
EH-IDTBR	-	-	3.69	17.88	-	-

<sup>a</sup>Calculation from OOP direction. <sup>b</sup>Calculation from IP direction. <sup>c</sup>The film is annealed by CF, for 15s.

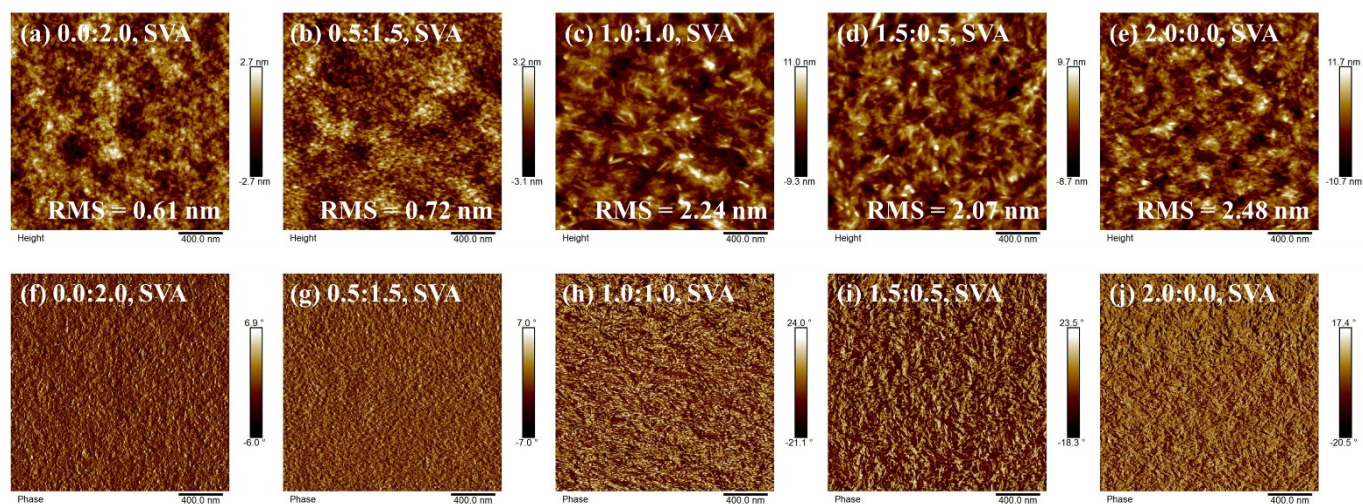


**Fig. S14** AFM height (top), phase (bottom) images of PTB7-Th:T2-ORH:EH-IDTBR ternary solar cells with different blend ratio for (a,f) 1.0:0.0:2.0, (b,g) 1.0:0.5:1.5, (c,h) 1.0:1.0:1.0, (d,i) 1.0:1.5:0.5, (e,j) 1.0:2.0:0.0.

**Table S7** Summary of photovoltaic characteristics of PTB7-Th:T2-OEH:EH-IDTBR and PTB7-Th:PC<sub>71</sub>BM (1.0:1.5) with different thermal stress temperature<sup>a</sup>

Acceptor	Annealing	$V_{oc}$ [V]	$J_{sc}$ [mA/cm <sup>2</sup> ]	FF [%]	PCE <sup>a</sup> [%]
T2-ORH:EH-IDTBR = 0.0:2.0	W/O	1.02	15.73	63	10.07
	90 °C, 20min	1.02	15.54	61	9.74
	120 °C, 20min	1.01	15.42	59	9.10
	150 °C, 20min	1.00	15.36	57	8.71
T2-ORH:EH-IDTBR = 1.0:1.0	W/O	1.05	17.51	63	11.55
	90 °C, 20min	1.04	17.73	61	11.27
	120 °C, 20min	1.04	17.21	62	11.15
	150 °C, 20min	1.02	16.74	61	10.44
T2-ORH:EH-IDTBR = 2.0:0.0	W/O	1.07	14.74	60	9.39
	90 °C, 20min	1.06	14.21	60	9.07
	120 °C, 20min	1.04	14.10	59	8.65
	150 °C, 20min	1.03	13.20	59	8.12

<sup>a</sup>The devices architecture is ITO/ZnO NPs/PEIE/photoactive layer( $d = \sim 100\text{nm}$ )/MoO<sub>x</sub>/Ag.

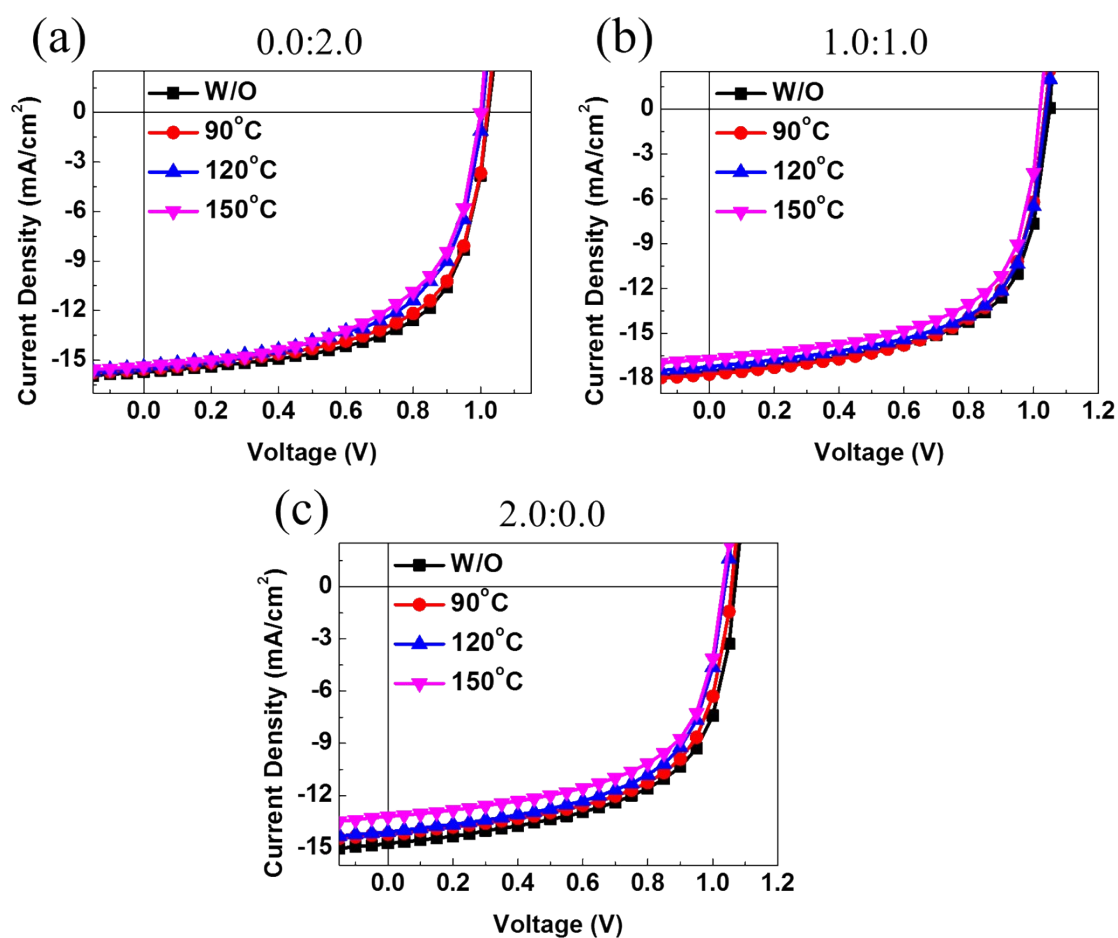


**Fig. S15** The  $J$ - $V$  curves of (a) PTB7-Th:T2-ORH:EH-IDTBR (1.0:0.0:2.0), (b) PTB7-Th:T2-ORH:EH-IDTBR (1.0:1.0:1.0), (c) PTB7-Th:T2-ORH:EH-IDTBR (1.0:2.0:0.0) OSCs with different thermal ageing temperature under the illumination of AM 1.5 G,  $100\text{ mW cm}^{-2}$ .

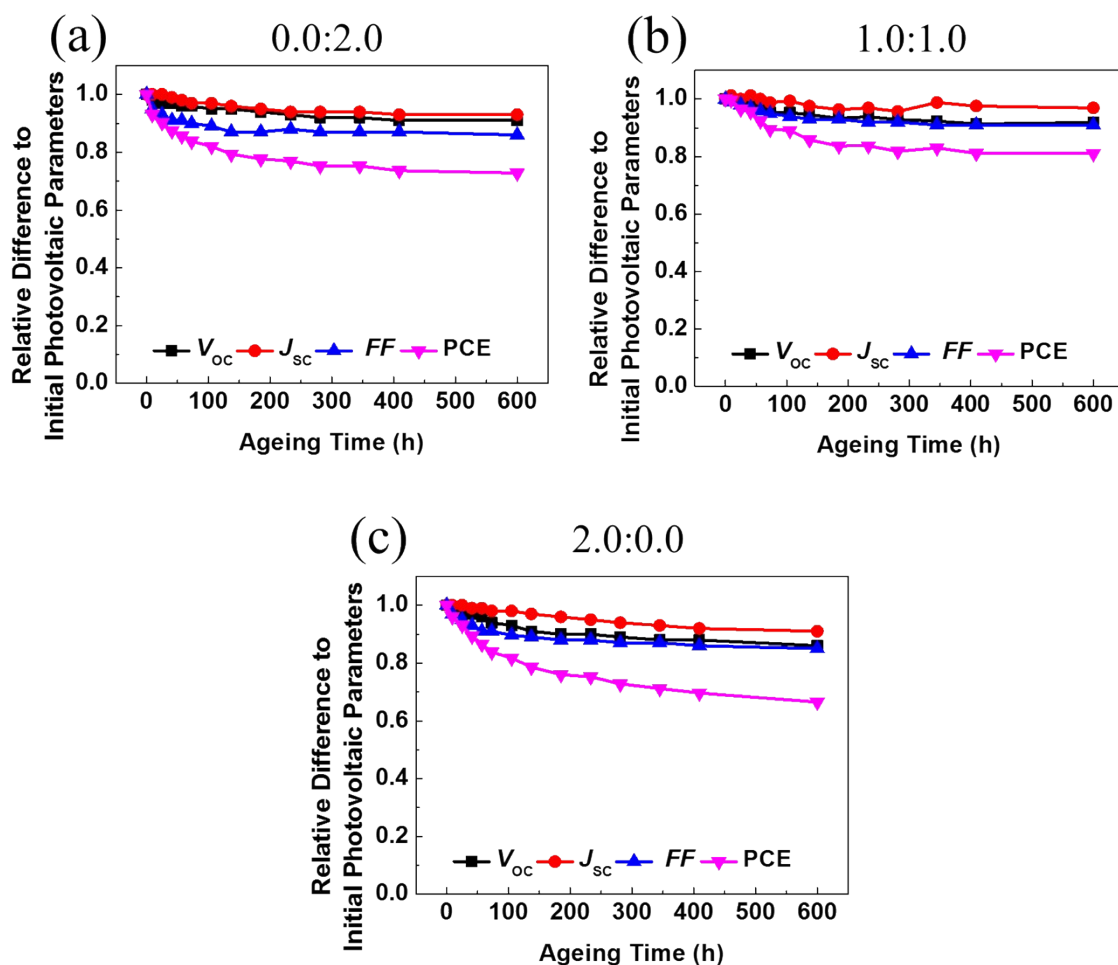


**Fig. S16** The  $J$ - $V$  curves of (a) PTB7-Th:T2-ORH:EH-IDTBR (1.0:0.0:2.0), (b) PTB7-Th:T2-ORH:EH-IDTBR (1.0:1.0:1.0), (c) PTB7-Th:T2-ORH:EH-IDTBR (1.0:2.0:0.0) OSCs with glass-to-glass encapsulated stored under one sun for 600h.

**Table S8** Photovoltaic characteristics of PTB7-Th:T2-ORH:EH-IDTBR and PTB7-Th:PC<sub>71</sub>BM (1.0:1.5) with process conditions in N<sub>2</sub> and air

Acceptor	Process	$V_{oc}$	$J_{sc}$	$FF$	$PCE^a$
		[V]	[mA/cm <sup>2</sup> ]	[%]	[%]
0.0:2.0	N <sub>2</sub>	1.02	15.73	63	10.07
	Air	1.01	15.58	61	9.61
1.0:1.0	N <sub>2</sub>	1.05	17.51	63	11.55
	Air	1.04	17.21	63	11.35
2.0:0.0	N <sub>2</sub>	1.07	14.74	60	9.39
	Air	1.05	14.45	57	8.66

<sup>a</sup>The devices architecture is ITO/ZnO NPs/PEIE/photoactive layer( $d = \sim 100\text{nm}$ )/MoO<sub>x</sub>/Ag.

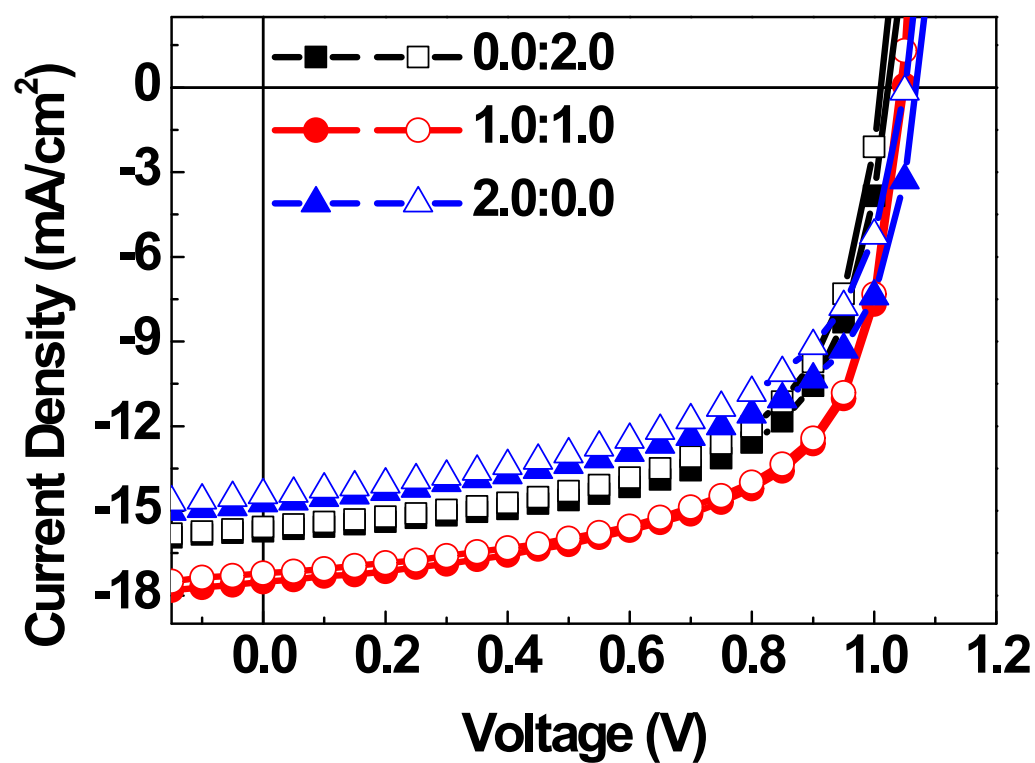


**Fig. S17** *J*–*V* characteristics of optimized OSCs fabricated in N<sub>2</sub> (full symbols) and air (open symbols) under simulated 1 sun illumination.

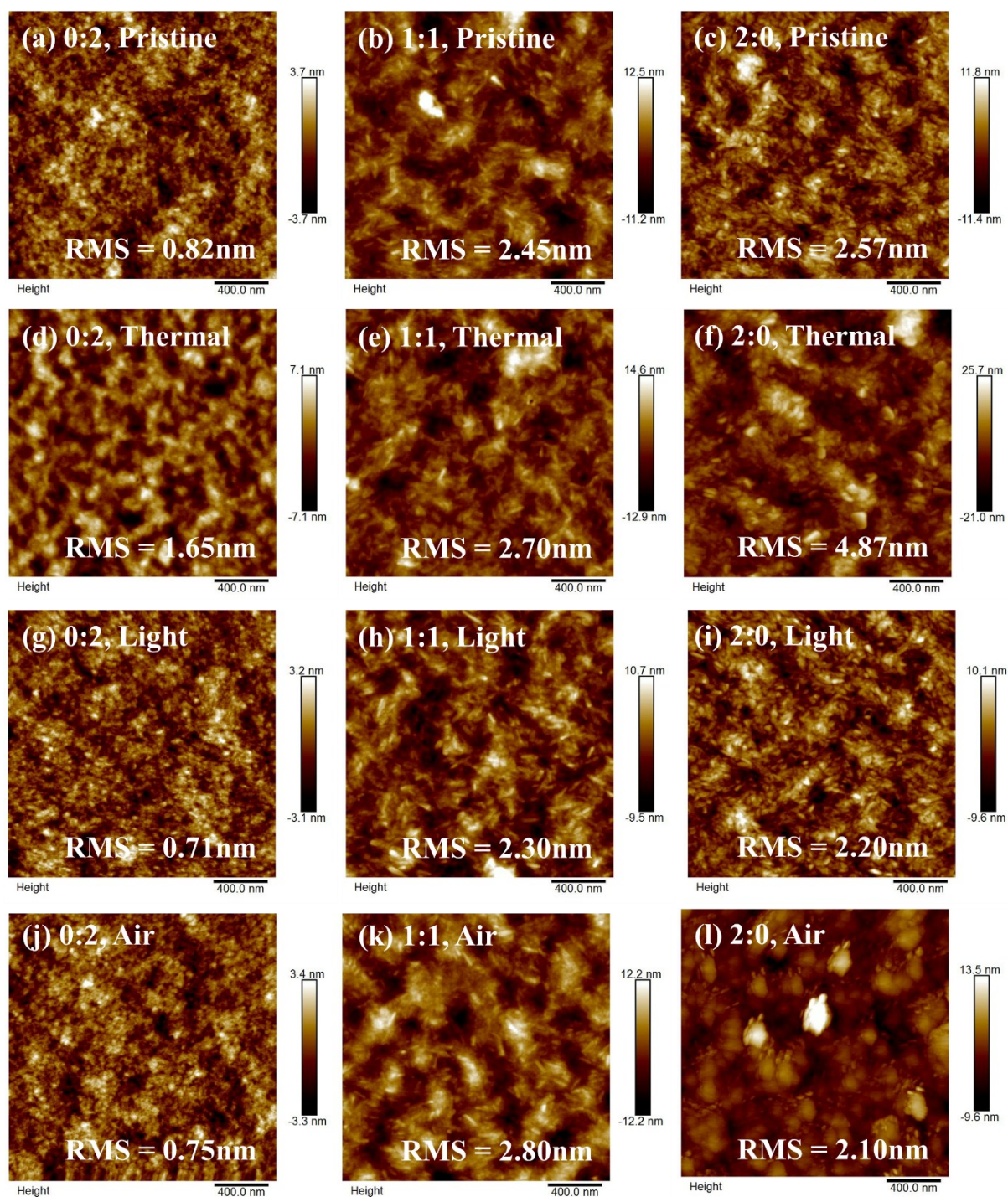


**Fig. S18** AFM images of PTB7-Th:T2-ORH:EH-IDTBR (1.0:0.0:2.0), PTB7-Th:T2-ORH:EH-IDTBR (1.0:1.0:1.0), PTB7-Th:T2-ORH:EH-IDTBR (1.0:2.0:0.0) with (a,b,c) pristine, (d,e,f) thermal annealing at 150 °C for 20 min, (g,h,i) photo exposure for 600 h, and (j,k,l) air-processed devices.

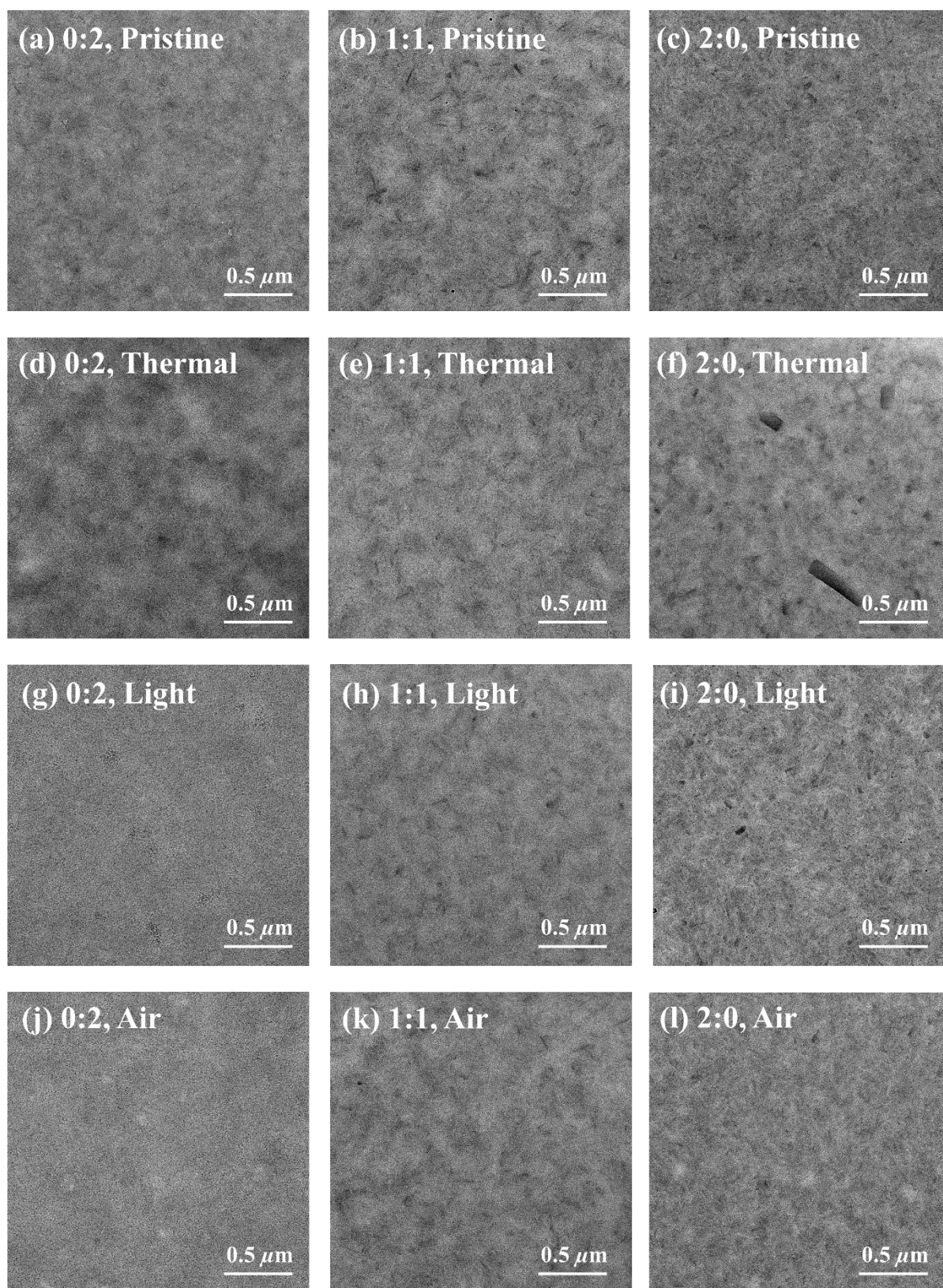


**Fig. S19** TEM images of PTB7-Th:T2-ORH:EH-IDTBR (1.0:0.0:2.0), PTB7-Th:T2-ORH:EH-IDTBR (1.0:1.0:1.0), PTB7-Th:T2-ORH:EH-IDTBR (1.0:2.0:0.0) with (a,b,c) pristine, (d,e,f) thermal annealing at 150 °C for 20 min, (g,h,i) photo exposure for 600 h, and (j,k,l) air-processed devices.

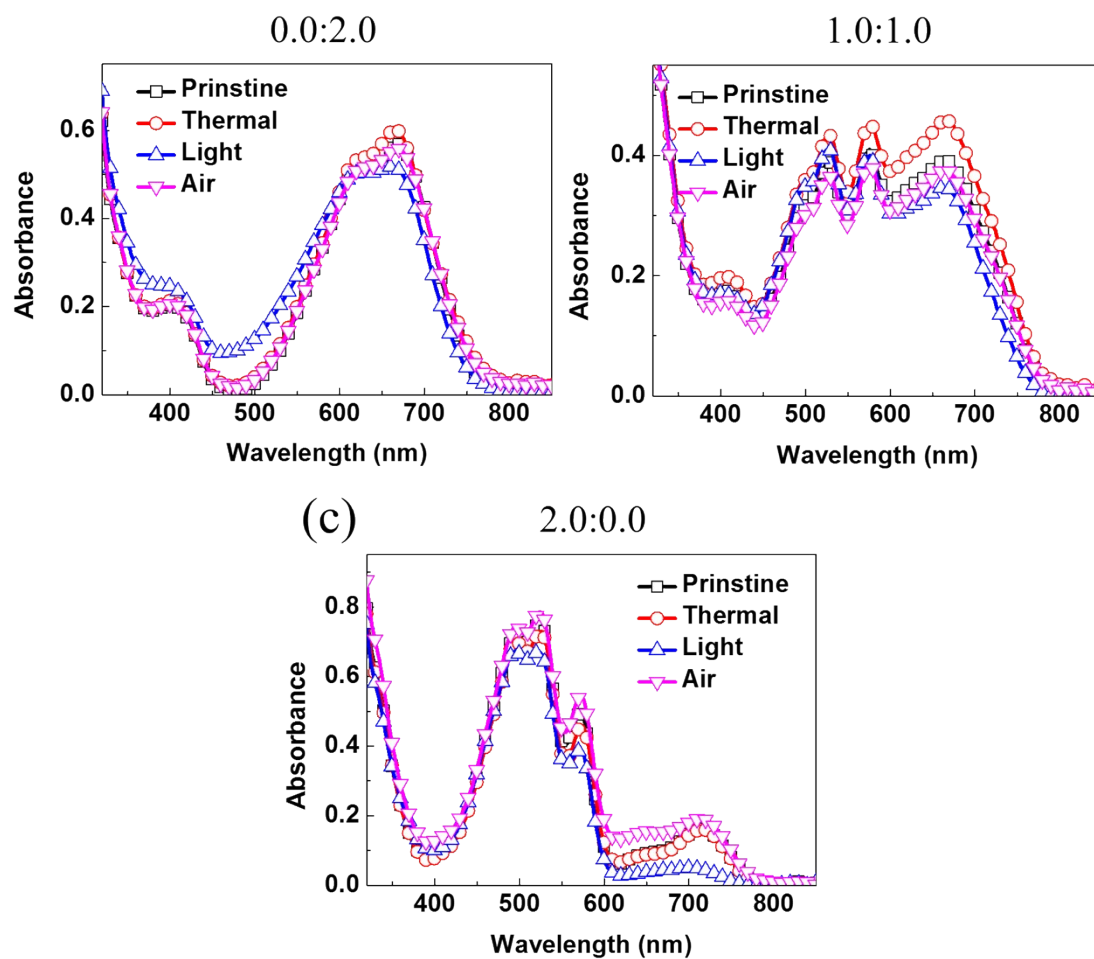


**Fig. S20** UV-vis absorption spectrum of (a) PTB7-Th:T2-ORH:EH-IDTBR (1.0:0.0:2.0), (b) PTB7-Th:T2-ORH:EH-IDTBR (1.0:1.0:1.0), (c) PTB7-Th:T2-ORH:EH-IDTBR (1.0:2.0:0.0) devices after stability tests, which is composed with glass/ITO/ZnO NPs/PEIE/photoactive layer.

**Table S9** Photovoltaic parameters of bottom, top and tandem cells

Photoactive Layer	Cell	$V_{oc}$ [V]	$J_{sc}$ [mA/cm <sup>2</sup> ]	FF [%]	PCE [%]
PTB7-Th: T2-ORH	Bottom <sup>a</sup>	1.06	13.65	61	8.84
PTB7-Th: EH-IDTBR	Top <sup>b</sup>	1.01	16.39	60	9.93
-	Tandem <sup>c</sup>	2.05 (2.04 ± 0.02) <sup>d</sup>	8.76 (8.60 ± 0.15) <sup>d</sup>	60 (58 ± 2) <sup>d</sup>	10.68 (10.39 ± 0.30) <sup>d</sup>

<sup>a</sup>The devices architecture is ITO/ZnO NPs/PEIE/PTB7-Th:T2-ORH( $d = \sim 100\text{nm}$ )/PEDOT:PSS/Ag and all devices are annealed by SVA using CF, for 15s.

<sup>b</sup>The devices architecture is ITO/ZnO NPs/PEIE/PTB7-Th:EH-IDTBR( $d = \sim 100\text{nm}$ )/MoO<sub>x</sub>/Ag.

<sup>c</sup>The devices architecture is ITO/ZnO NPs/PEIE/PTB7-Th:T2-ORH( $d = \sim 100\text{nm}$ )/PEDOT:PSS/ZnO NPs/PEIE/PTB7-Th:EH-IDTBR( $d = \sim 100\text{nm}$ )/MoO<sub>3</sub>/Ag.

<sup>d</sup>The average photovoltaic parameters in the brackets are obtained from over 10 independent tandem devices.

Device ID : OPV #2  
Date of Test : December 29, 2016  
Simulator : WACOM, WXS-155S-L2 (Class-AAA)  
Reference solar cell : KIER-PS-FD #1  
Test condition : STC (AM1.5G, 100 mW/cm<sup>2</sup>, 25.0 ± 1.0 °C)  
Device Area : 0.04 cm<sup>2</sup> (자광 마스크 적용 면적)  
Sample Type : Tandem organic solar cell (glass plate based)

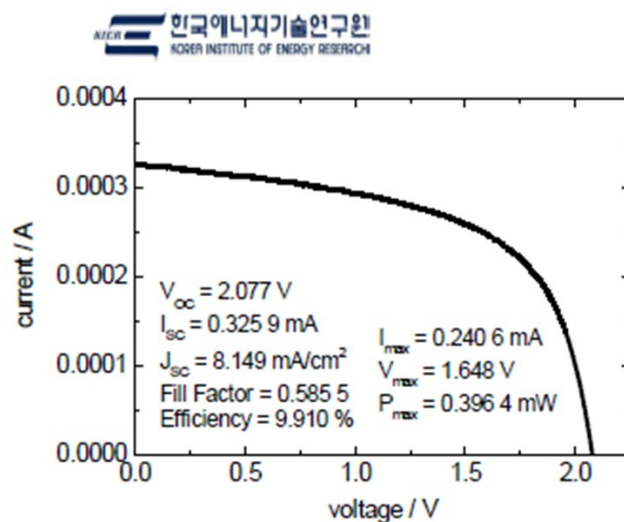


**Fig. S21** *I-V* curve and photovoltaic parameters of the optimum tandem OSC certified by the Korea Institute of Energy Research (KIER).

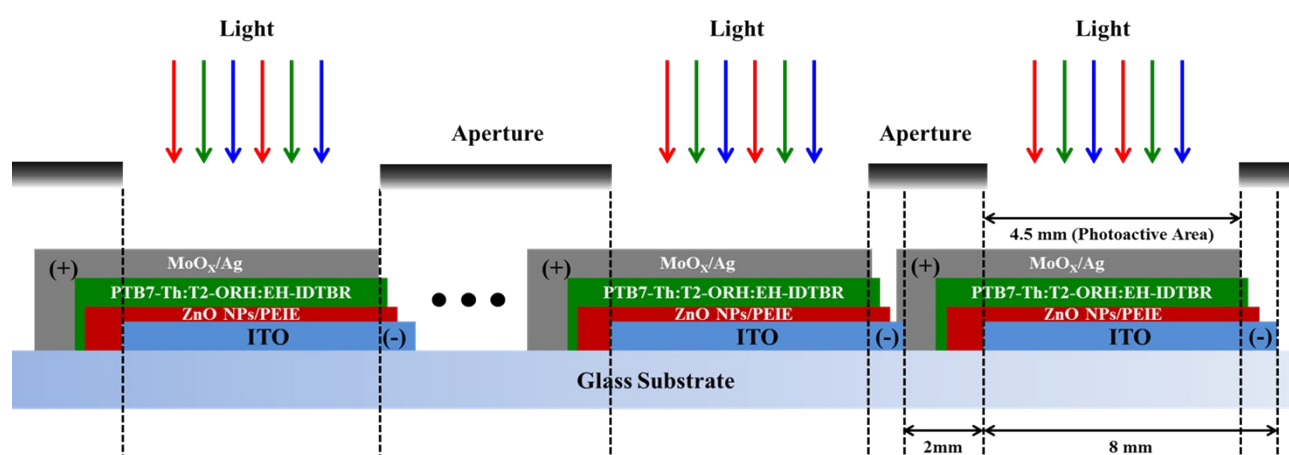
**Table S10** Photovoltaic parameters of sub-module ternary-blend OSCs<sup>a</sup>

Stripes	Aperture Size	GF <sup>b</sup>	V <sub>oc</sub> [V]	J <sub>sc</sub> [mA/cm <sup>2</sup> ]	FF [%]	PCE [%]
6	13.5 cm <sup>2</sup>	54 %	6.36 (6.13 ± 0.21) <sup>c</sup>	2.83 (2.70 ± 0.12) <sup>c</sup>	56 (53 ± 3) <sup>c</sup>	10.08 (9.79 ± 0.30) <sup>c</sup>

<sup>a</sup>The sub-module device is ITO/ZnO NPs/PEIE/photoactive layer( $d = \sim 100\text{nm}$ )/MoO<sub>x</sub>/Ag and comprise a serial connection of 6 stripes.

<sup>b</sup>GF is geometric FF.

<sup>c</sup>The average photovoltaic parameters in the brackets are obtained from over 10 sub-module OSCs.

**Fig. S22** Schematic diagram of sub-module device architecture.

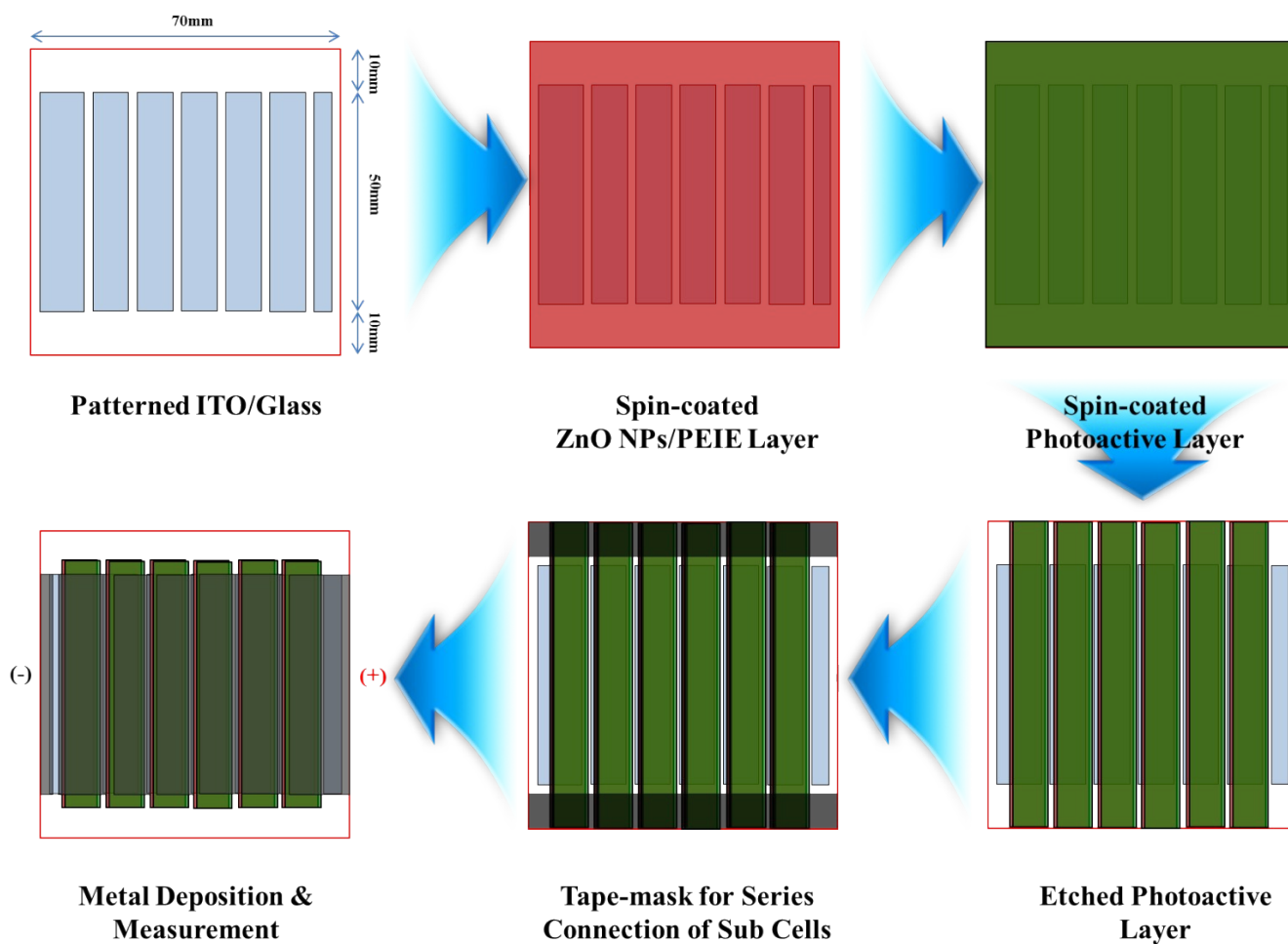


**Fig. S23** Schematic diagram for preparing sub-module OSCs.

**Table S11** Summarized photovoltaic parameters of reported high-efficiency sub-module OSCs

Photoactive Layer	Cells	Photoactive Area	Photovoltaic Properties	Reference
PTB7-Th: PC <sub>71</sub> BM	3	16.6 cm <sup>2</sup>	$V_{OC} = 2.37V$ , $J_{SC} = 4.87\text{mA/cm}^2$ , $FF = 58\%$ , PCE = 6.70%	2
P3HT: PC <sub>60</sub> BM	20	57.0 cm <sup>2</sup>	$V_{OC} = 11.70V$ , $J_{SC} = 32.8\text{mA}$ , $FF = 51\%$ , PCE = 3.14%	3
PBTZT-stat- BDTT-8: PC <sub>61</sub> BM	4	35.0 cm <sup>2</sup>	$V_{OC} = 10.50V$ , $J_{SC} = 0.63\text{mA/cm}^2$ , $FF = 62\%$ , PCE = 5.28%	4
D5A: PC <sub>71</sub> BM	11	62.7 cm <sup>2</sup>	$V_{OC} = 9.94V$ , $J_{SC} = 1.14\text{mA/cm}^2$ , $FF = 61\%$ , PCE = 6.54%	5
PDTT-BOBT: PC <sub>71</sub> BM	11	66.7 cm <sup>2</sup>	$V_{OC} = 8.66V$ , $J_{SC} = 1.20\text{mA/cm}^2$ , $FF = 53\%$ , PCE = 5.44%	6
BDT2: PC <sub>71</sub> BM	11	77.8 cm <sup>2</sup>	$V_{OC} = 10.00V$ , $J_{SC} = 1.08\text{mA/cm}^2$ , $FF = 69\%$ , PCE = 7.45%	7
P3HT: IDTBR	12	59.5 cm <sup>2</sup>	$V_{OC} = 8.53V$ , $J_{SC} = 53.90\text{mA}$ , $FF = 64\%$ , PCE = 5.00%	8
PTB7-Th : p-DTS(FBTTH) <sub>2</sub> : PC <sub>71</sub> BM	4	20.0 cm <sup>2</sup>	$V_{OC} = 2.71V$ , $J_{SC} = 3.89\text{mA/cm}^2$ , $FF = 49\%$ , PCE = 5.18%	9
PBTIBDTT: ITIC-F	4	3.5 cm <sup>2</sup>	$V_{OC} = 4.53V$ , $J_{SC} = 2.92\text{mA/cm}^2$ , $FF = 65\%$ , PCE = 8.60%	10
<b>PTB7-Th: T2-ORH: EH-IDTBR</b>	<b>6</b>	<b>13.5 cm<sup>2</sup></b>	<b><math>V_{OC} = 6.36V</math>, <math>J_{SC} = 2.83\text{mA/cm}^2</math>, <math>FF = 56\%</math>, PCE = 10.08%</b>	<b>in this work</b>

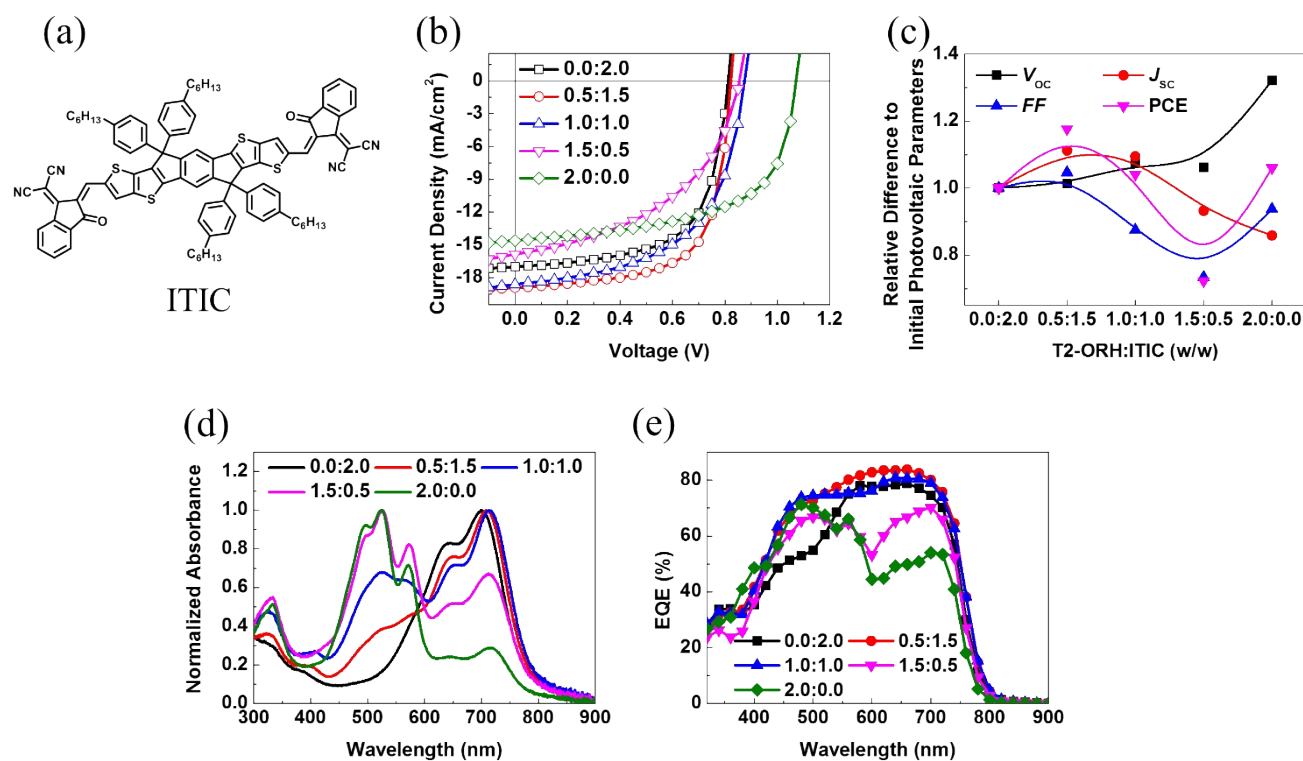


**Fig. S24** (a) Chemical structures of non-fullerene acceptor, ITIC. (b)  $J$ - $V$  characteristics, (c) relative changes of photovoltaic parameters, (d) normalized absorption spectrum and (e) EQE curves in PTB7-Th-based ternary-blend OSCs with different T2-ORH:ITIC blend ratio.

The incorporation of the T2-ORH NFA could also improve the photovoltaic performance in other ternary-blend systems with ITIC as a host acceptor. By adding of T2-ORH into the PTB7-Th:ITIC binary film, it can covers a broad absorption range from 300 to 800 nm. The PCE of ternary-blend OSCs reaches 10.37% with 0.5:1.5 blend ratio in T2-ORH:ITIC, resulting from a simultaneously increased  $J_{SC}$  of  $18.92 \text{ mA cm}^{-2}$ ,  $FF$  of 67% and  $V_{OC}$  of 0.82 V. Even though it shows slightly decreased PCE as compared with PTB7-Th:T2-ORH:EH-IDTBR ternary-blend OSCs, the incorporation of third component, T2-ORH promote the PCE enhancement from the binary devices (PTB7-Th:ITIC = 8.81%, PTB7-Th:T2-ORH = 9.34%).

**Table S12** Photovoltaic parameters of PTB7-Th-based ternary-blend OSCs with different T2-ORH contents in the acceptors<sup>a</sup>

Acceptor	$V_{oc}$ [V]	$J_{sc}$ [mA/cm <sup>2</sup> ]	$FF$ [%]	PCE [%]	$\mu_h$ [cm <sup>2</sup> /V s] <sup>d</sup>	$\mu_e$ [cm <sup>2</sup> /V s] <sup>e</sup>
T2-ORH:ITIC =0.0:2.0	0.81	17.01 (16.41) <sup>b</sup>	64	8.81 (8.53 ± 0.28) <sup>c</sup>	4.47 × 10 <sup>-4</sup>	5.86 × 10 <sup>-5</sup>
T2-ORH:ITIC =0.5:1.5	0.82	18.92 (18.30) <sup>b</sup>	67	10.37 (10.05 ± 0.33) <sup>c</sup>	7.51 × 10 <sup>-4</sup>	5.69 × 10 <sup>-5</sup>
T2-ORH:ITIC =1.0:1.0	0.87	18.62 (17.86) <sup>b</sup>	56	9.17 (8.98 ± 0.20) <sup>c</sup>	6.47 × 10 <sup>-4</sup>	1.59 × 10 <sup>-5</sup>
T2-ORH:ITIC =1.5:0.5	0.86	15.86 (14.87) <sup>b</sup>	47	6.37 (6.10 ± 0.27) <sup>c</sup>	3.26 × 10 <sup>-4</sup>	1.26 × 10 <sup>-6</sup>
T2-ORH:ITIC =2.0:0.0	1.07	14.61 (13.40) <sup>b</sup>	60	9.34 (9.00 ± 0.35) <sup>c</sup>	8.12 × 10 <sup>-4</sup>	2.51 × 10 <sup>-7</sup>

<sup>a</sup>Inverted device architecture is ITO/ZnO NPs/PEIE/photoactive layer( $d = \sim 100\text{nm}$ )/MoO<sub>x</sub>/Ag and all photoactive layers are annealed by solvent vapor annealing (SVA) using DCM, for 15s.

<sup>b</sup>The value is calculated from EQE data.

<sup>c</sup>The average photovoltaic parameters in the brackets are obtained from over 20 independent devices.

<sup>d</sup>Hole-only device is ITO/PEDOT:PSS/photoactive layer( $d = \sim 100\text{nm}$ )/Au.

<sup>e</sup>Electron-only device is ITO/ZnO NPs/PEIE/photoactive layer( $d = \sim 100\text{nm}$ )/Ca/Al.

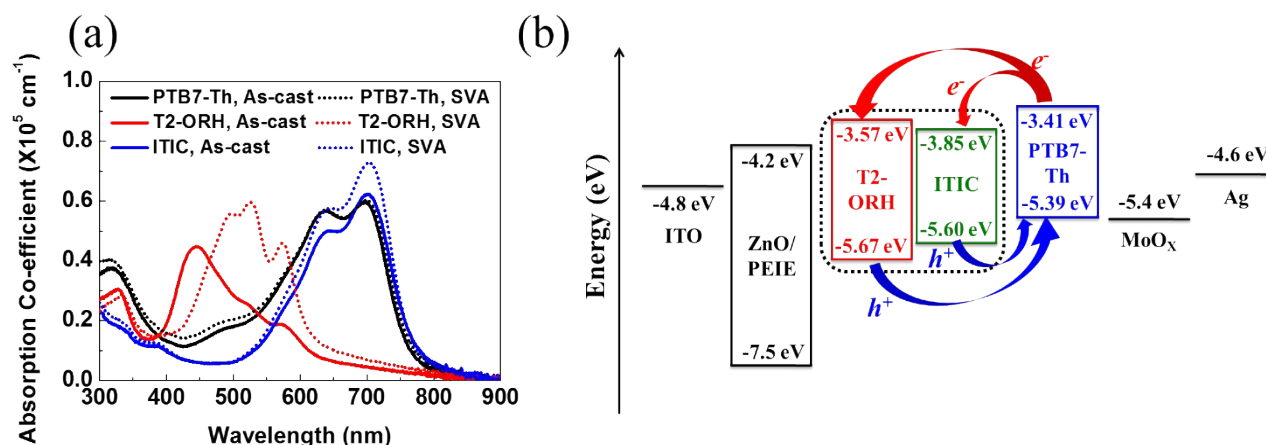


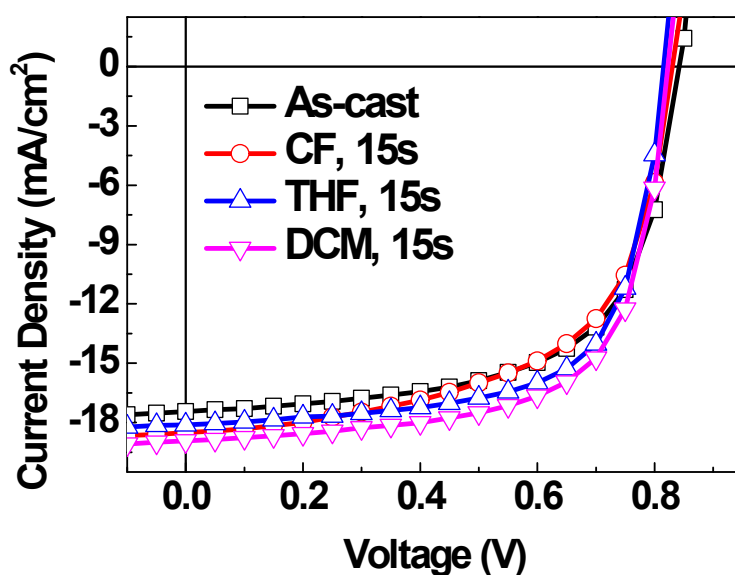
**Fig. S25** (a) Absorption coefficient of donor and acceptors with as-cast and SVA (DCM, 15s) in the film state. (b) Energy-level diagram of used photoactive materials in ternary-blend OSCs.

The PTB7-Th and ITIC film exhibits a wide photon harvesting range from 300 to 800 nm with a major absorption peak around 700 nm, whereas the T2-ORH film shows a strong photon harvesting ability in the short wavelength range with 400-600 nm. The absorption spectra for these materials are obviously complementary, which may provide great potential for the enhanced  $J_{sc}$  value in ternary-blend OSCs.

**Table S13** Photovoltaic properties of ternary-blend OSCs with different solvent vapor annealing systems under AM 1.5G illumination<sup>a</sup>

Photoactive Layer	Annealing	$V_{oc}$ [V]	$J_{sc}$ [mA/cm <sup>2</sup> ]	$FF$ [%]	PCE [%]
T2-ORH:ITIC =0.5:1.5	As-cast	0.84	17.45	63	9.27
	CF, 15s	0.83	18.50	59	9.10
	THF, 15s	0.82	18.11	67	9.93
	DCM, 15s	0.82	18.92	67	10.37

<sup>a</sup>Inverted device architecture is ITO/ZnO NPs/PEIE/photoactive layer( $d = \sim 100\text{nm}$ )/MoO<sub>x</sub>/Ag.

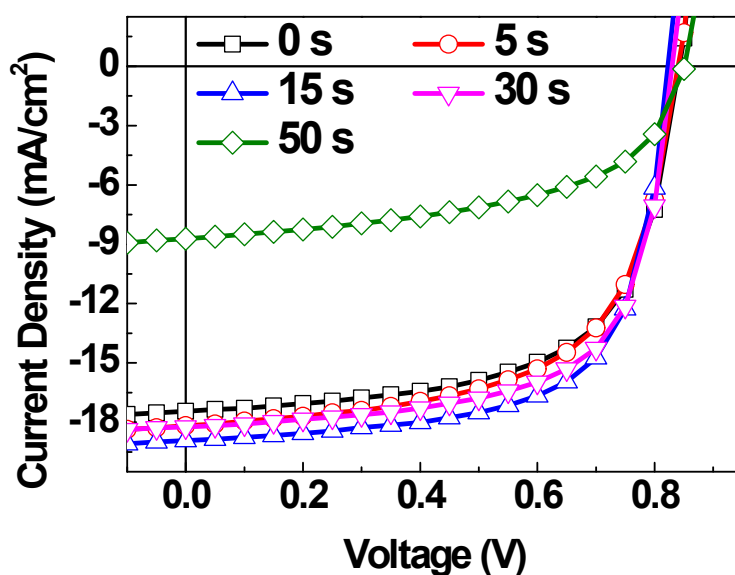
**Fig. S26**  $J$ - $V$  curves of PTB7-Th:T2-ORH:ITIC-based ternary-blend OSCs with various vapor annealing solvent.

To find out the best solvent for SVA, the ternary-blend photoactive films were annealed by various solvents. The best efficiency is produced from dichloromethane (DCM, CH<sub>2</sub>Cl<sub>2</sub>).

**Table S14** Photovoltaic properties of PTB7-Th:T2-ORH:ITIC (1.0:0.5:1.5) ternary-blend OSCs with various CH<sub>2</sub>Cl<sub>2</sub> vapor annealing time under AM 1.5G illumination<sup>a</sup>

SVA Time [s]	V <sub>oc</sub> [V]	J <sub>sc</sub> [mA/cm <sup>2</sup> ]	FF [%]	PCE [%]
0	0.84	17.45	63	9.27
5	0.84	18.17	62	9.40
15	0.82	18.92	67	10.37
30	0.83	18.23	66	9.99
50	0.85	8.73	53	3.97

<sup>a</sup>Inverted device architecture is ITO/ZnO NPs/PEIE/photoactive layer( $d = \sim 100\text{nm}$ )/MoO<sub>x</sub>/Ag and SVA is conducted by DCM.

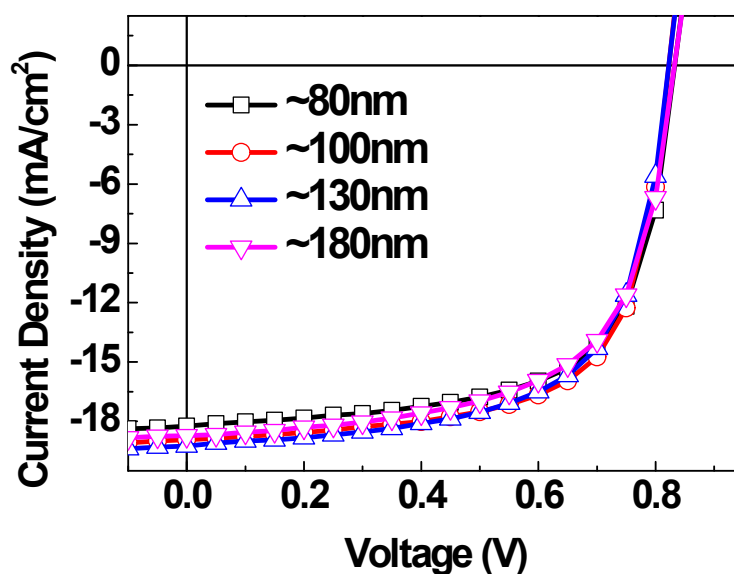
**Fig. S27**  $J$ - $V$  curves of PTB7-Th:T2-ORH:ITIC-based ternary-blend OSCs with different solvent vapor annealing time.

We investigated the photovoltaic parameters of PTB7-Th:T2-ORH:ITIC-based ternary-blend OSCs as a function of SVA time. SVA was varied between 0-50 s, allowing to control and improve the molecular packing and morphological properties with respect to performance in ternary-blend OSCs. The maximum PCE is found to 15 s of SVA with DCM solvent.

**Table S15** Photovoltaic properties of PTB7-Th:T2-ORH:ITIC (1.0:0.5:1.5) with different photoactive layer thickness under AM 1.5G illumination<sup>a</sup>

Thickness [nm]	$V_{oc}$ [V]	$J_{sc}$ [mA/cm <sup>2</sup> ]	$FF$ [%]	PCE [%]
~180	0.83	18.72	63	9.85
~130	0.82	19.25	64	10.19
~100	0.82	18.92	67	10.37
~80	0.83	18.23	66	9.97

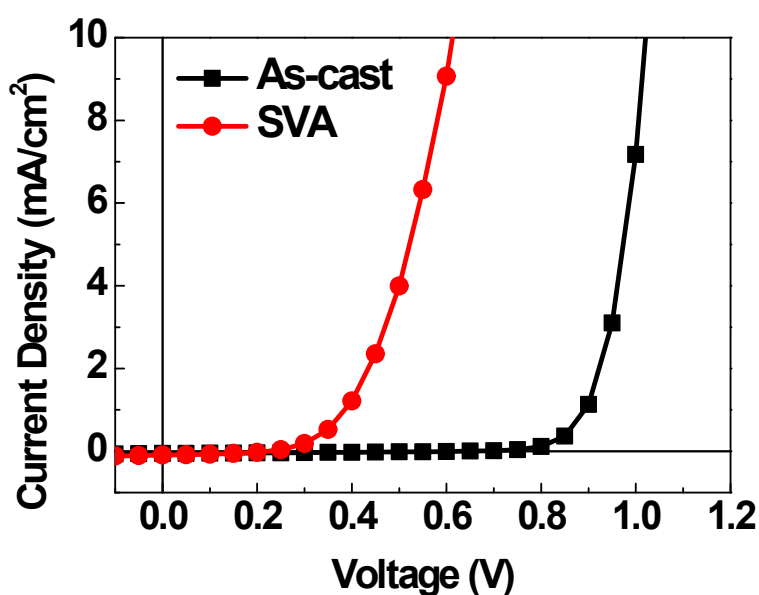
<sup>a</sup>Inverted device architecture is ITO/ZnO NPs/PEIE/photoactive layer( $d = \sim 100\text{nm}$ )/MoO<sub>x</sub>/Ag and all photoactive layers are annealed by SVA(DCM, 15s).

**Fig. S28**  $J$ - $V$  curves of PTB7-Th:T2-ORH:ITIC-based ternary-blend OSCs with different photoactive layer thickness.

**Table S16** Photovoltaic properties of T2-ORH:ITIC (0.5:1.5)-based devices with as-cast and solvent vapor annealing under AM 1.5G illumination<sup>a</sup>

Annealing	$V_{oc}$ [V]	$J_{sc}$ [mA/cm <sup>2</sup> ]	$FF$ [%]	PCE [%]
As-cast	0.64	0.06	30	0.01
SVA	0.22	0.09	40	0.01

<sup>a</sup>Inverted device architecture is ITO/ZnO NPs/PEIE/photoactive layer( $d = \sim 100\text{nm}$ )/MoO<sub>x</sub>/Ag and SVA is conducted by SVA(DCM, 15s).

**Fig. S29**  $J$ - $V$  curves for the devices based on T2-ORH:ITIC (0.5:1.5) with as-cast (black) and SVA (red) under AM 1.5G illumination with a light intensity of  $100\text{ mW cm}^{-2}$ .

We fabricated devices with T2-ORH:ITIC (0.5:1.5, w/w) as binary OSCs. Both of as-cast and SVA devices do not contribute to the photovoltaic effects.

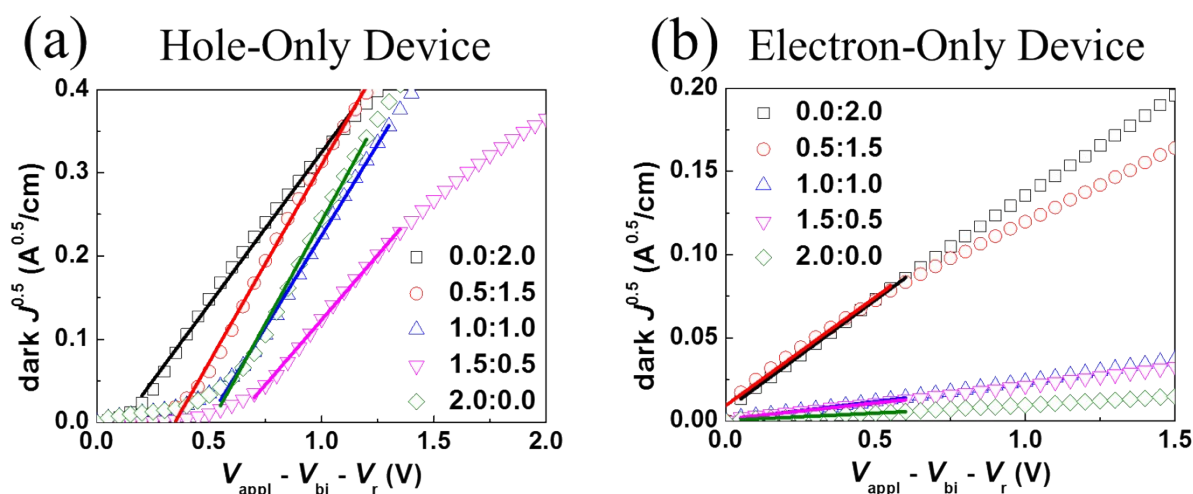


**Fig. S30**  $J$ - $V$  characteristics from (a) the hole-only and (b) the electron-only devices based on PTB7-Th:T2-ORH:ITIC ternary-blend films.

To understand the relationship between charge transport and photovoltaic properties, the hole and electron mobility of the ternary-blend films were measured from space charge limited current (SCLC) method. For the PTB7-Th:T2-ORH:ITIC devices, the hole mobility follows a similar trend and only drops in the T2-ORH:ITIC (1.5:0.5, w/w) blend ratio. And the electron mobility of ternary-blend films monotonically decreases with increase in concentration of T2-ORH. Note is that the hole and electron mobility of the optimum blend ratio (T2-ORH:ITIC = 0.5:1.5, w/w) were  $7.51 \times 10^{-4}/5.69 \times 10^{-5} \text{ cm}^2/\text{V s}$ , which could allow the photo-induced charge carriers to be efficiently collected by respective electrode in the ternary-blend OSCs.

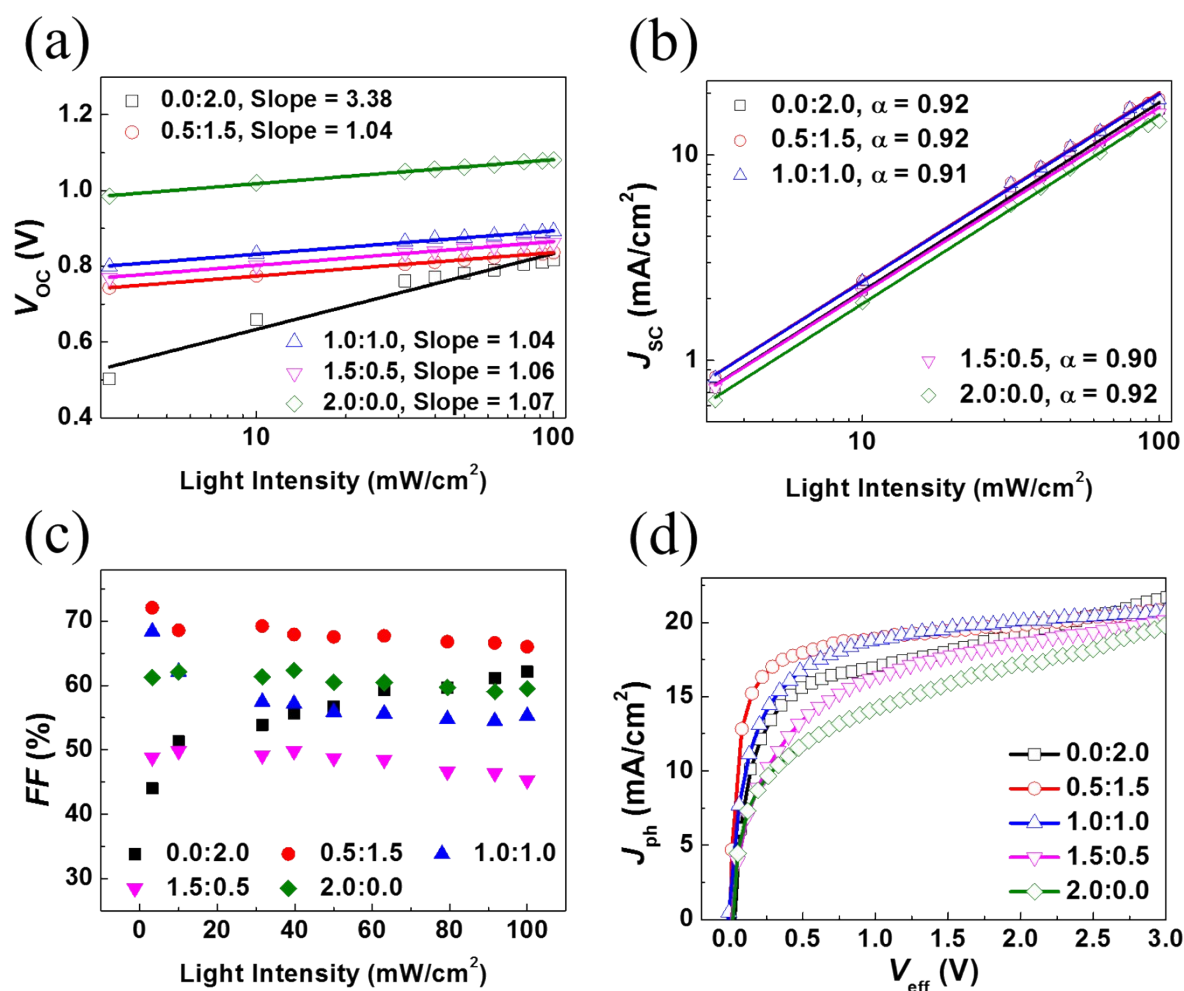


**Fig. S31** Light intensity dependence of (a)  $V_{oc}$ , (b)  $J_{sc}$ , (c)  $FF$ , and (d) photocurrent density dependence on the effective voltage of the PTB7-Th:T2-ORH:ITIC-based ternary-blend OSCs.

To gain a better understanding of the relationship between the charge recombination and photovoltaic properties, the dependence of the  $V_{oc}$ ,  $J_{sc}$ , and  $FF$  characteristics on the light intensity was examined. A plot of  $V_{oc}$  as a function of the light intensity based on  $V_{oc} \propto nkT/q \ln(P)$ , where  $k$  is the Boltzmann constant,  $T$  is the temperature in kelvin,  $q$  is the elementary charge and  $P$  is the light intensity. For a trap-assisted recombination system, a slope of  $2kT/q$  is obtained. In contrast, a value close to unity for  $n$  is estimated such that bimolecular recombination are the main mechanism of charge carrier recombination. The best ternary-blend OSCs (PTB7-Th:T2-ORH:ITIC = 1.0:0.5:1.5) show the slope of

$1.04kT/q$ , which demonstrate trap-assisted recombination is negligible. As shown in Fig. S24b,  $J_{SC}$  is presented as a function of the light intensity. The curve was fitted according to the power-law dependence of  $J_{SC}$  on the light intensity. It can be carried out by solving  $J_{SC} \propto P_{light}^{\alpha}$ , where the value of the power law scaling exponent  $\alpha$  indicates the strength of the bimolecular recombination. The more  $\alpha$  approaches unity, the possibility of bimolecular recombination is lower. The low value of  $\alpha$  (0.90) was obtained with the PTB7-Th:T2-ORH:ITIC (1.0:1.5:0.5) compared to the other ternary-blend OSCs, indicating the increased possibility of bimolecular recombination losses leading to the decline of the  $J_{SC}$  and  $FF$  values. In order to investigate the cause of the high  $FF$  in the PTB7-Th:T2-ORH:ITIC (1.0:0.5:1.5) ternary-blend OSCs, a qualitative study was undertaken of  $FF$  as a function of the light intensity (Fig. S24c). PTB7-Th:T2-ORH:ITIC (1.0:0.5:1.5) ternary-blend OSCs yielded the highest  $FF$  values at nearly all light intensities, indicating that it was capable of the most efficient charge extraction and transport to the respective electrode with the fewer charge recombination. To demonstrate that, the photocurrent density ( $J_{ph}$ ) as a function of the effective voltage ( $V_{eff}$ ) is plotted in Fig. S24d. For the PTB7-Th:T2-ORH:ITIC (1.0:0.5:1.5) ternary-blend system,  $J_{ph}$  shows nearly linear dependence on the effective voltage, reaching saturation at a low value of  $V_{eff}$  suggesting that the photo-induced excitons are efficiently dissociated into free carriers and extracted to the respective electrode as compared to the binary and other ternary-blend OSCs.

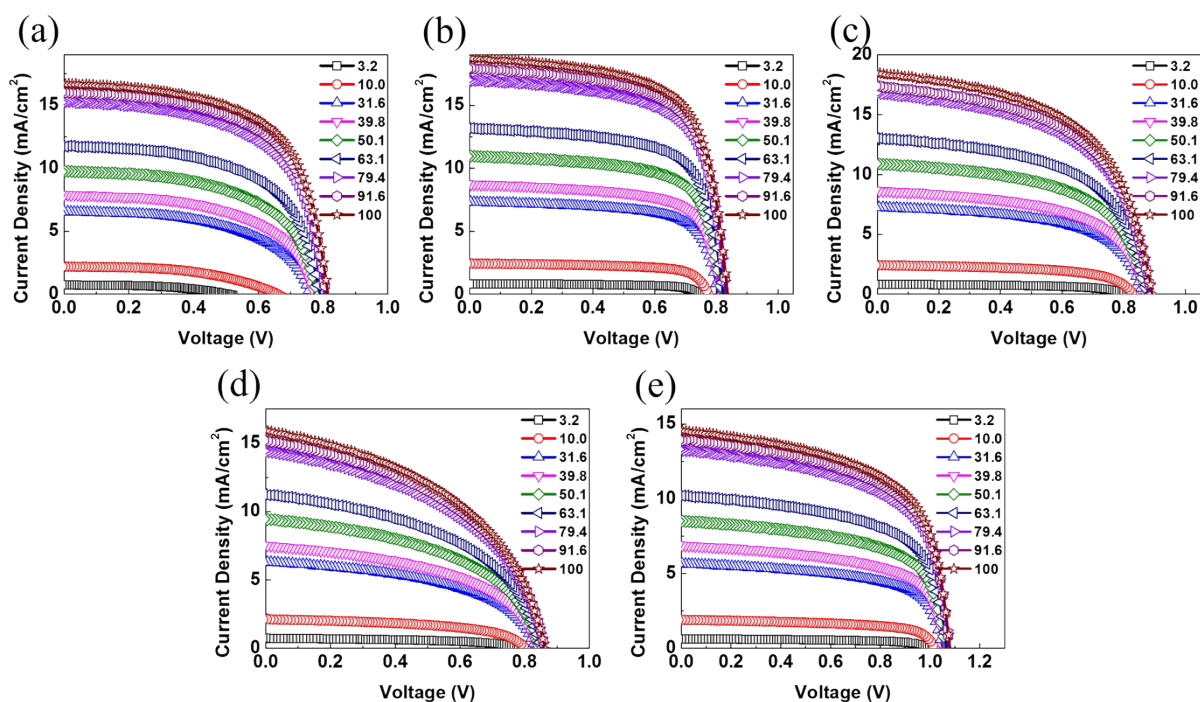


**Fig. S32** Light intensity-dependent  $J$ - $V$  curves of PTB7-Th-based ternary-blend OSCs for the (a) 0.0:2.0 (T2-ORH:ITIC), (b) 0.5:1.5 (T2-ORH:ITIC), (c) 1.0:1.0 (T2-ORH:ITIC), (d) 1.5:0.5 (T2-ORH:ITIC) and (e) 2.0:0.0 (T2-ORH:ITIC) acceptor blend ratio.

The correlation between the charge recombination kinetics and performance of ternary-blend OSCs was studied by investigating the dependence of certain  $J$ - $V$  characteristics on the light intensity.  $J$ - $V$  graphs of ternary-blend OSCs with different acceptor ratio subjected to light intensities varying from 3.2 to 100  $\text{mW cm}^{-2}$  are shown in Fig. S25. For the ternary-blend OSC with 1.0:0.5:1.5 (PTB7-Th:T2-ORH:ITIC), the  $J_{\text{ph}}$  was quickly saturated at all light intensities, thus demonstrating more efficient charge transfer and transport. However, the binary and other ternary-blend OSCs exhibit slower saturation at higher illumination intensities, indicating more recombination near the  $V_{\text{oc}}$ .

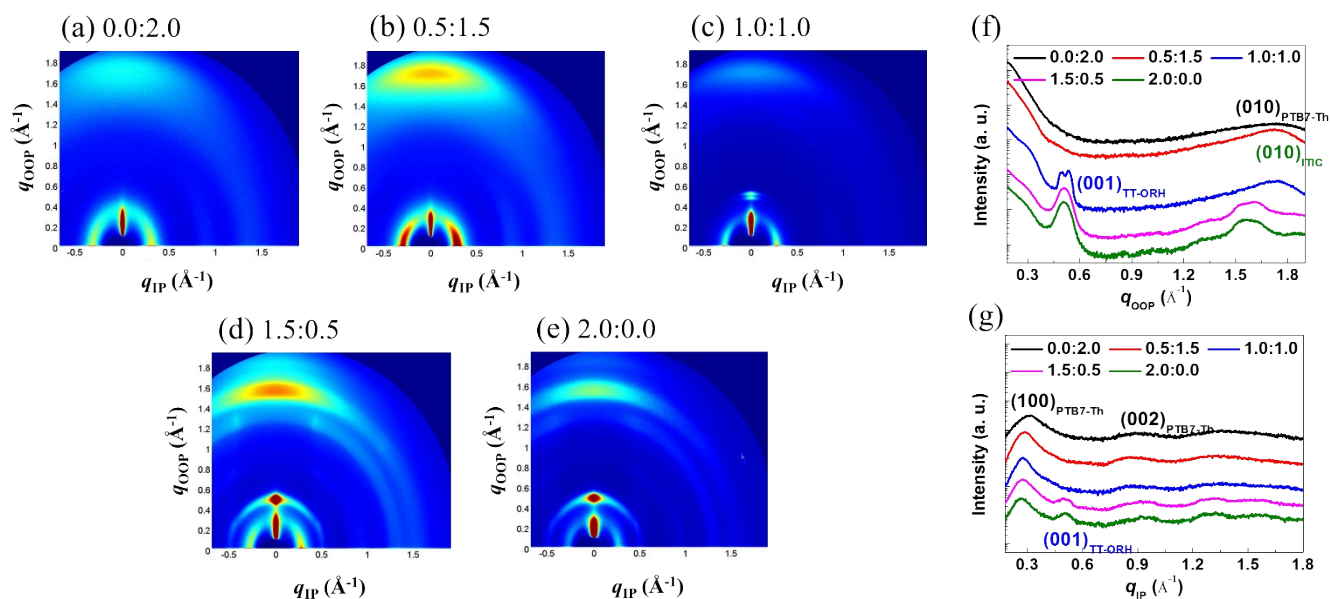


**Fig. S33** 2D GIWAXS patterns of ternary-blend films with different compositions based on (a) 1.0:0.0:2.0 (PTB7-Th:T2-ORH:ITIC), (b) 1.0:0.5:1.5 (PTB7-Th:T2-ORH:ITIC), (c) 1.0:1.0:1.0 (PTB7-Th:T2-ORH:ITIC), (d) 1.0:1.5:0.5 (PTB7-Th:T2-ORH:ITIC) and (e) 1.0:2.0:0.0 (PTB7-Th:T2-ORH:ITIC). One-dimensional integrated scattering profiles for the corresponding films (f) out-of plane and (g) in-plane direction.

In the 2D GIWAXS pattern for the PTB7-Th:ITIC (1:2) binary blend film (Fig. S26a), a broad  $\pi$ - $\pi$  scattering peak in the OOP direction is observed contributed from PTB7-Th and ITIC component, whereas the pattern of PTB7-Th:T2-ORH (1:2) blend film (Fig. S26e) exhibits more distinct (001) diffraction peak in both of OOP and IP direction from T2-ORH component. In the ternary-blend films (1.0:0.5:1.5), both of OOP (010)  $\pi$ - $\pi$  stacking and IP (100) lamellar diffraction peak become sharper, indicating enhanced coherence length for the PTB7-Th and ITIC component. This implies that T2-ORH is well inter-mixed into host donor and acceptor and improved molecular packing properties in ternary-blend systems. Therefore, the T2-ORH NFA induces favorable morphology for effective charge transport and generates well-intermixing with donor and acceptor like a carrier transport bridge.

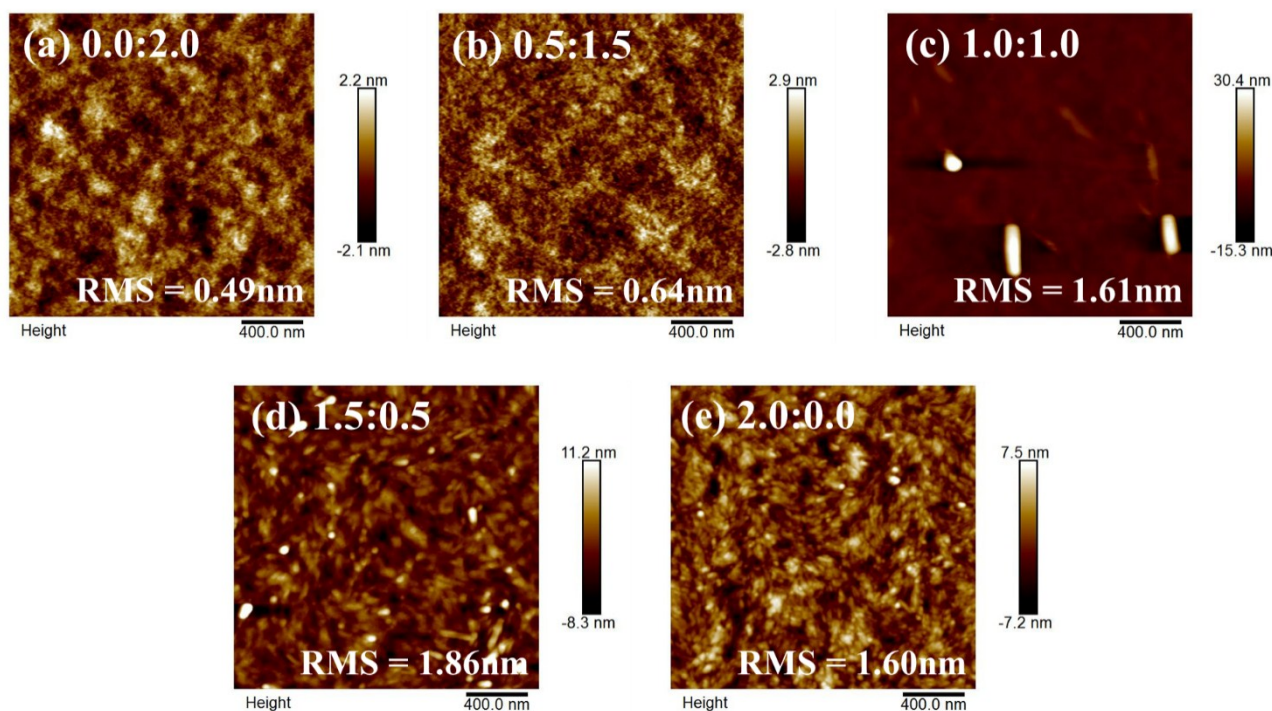


**Fig. S34** AFM images of ternary-blend photoactive layers with different blend ratio for (a) 1.0:0.0:2.0 (PTB7-Th:T2-ORH:ITIC), (b) 1.0:0.5:1.5 (PTB7-Th:T2-ORH:ITIC), (c) 1.0:1.0:1.0 (PTB7-Th:T2-ORH:ITIC), (d) 1.0:1.5:0.5 (PTB7-Th:T2-ORH:ITIC) and (e) 1.0:2.0:0.0 (PTB7-Th:T2-ORH:ITIC).

As shown AFM images in Fig. S27, the homogeneous morphologies of the PTB7-Th:T2-ORH:ITIC (1.0:0.5:1.5) blend films were observed, showing a RMS value of 0.64 nm, which is little increase compared with binary system (PTB7-Th:ITIC) due to the incorporation of high crystalline T2-ORH. In PTB7-Th:T2-ORH:ITIC (1.0:1.0:1.0) photoactive layers, the bright square-shaped parts are obtained related with T2-ORH domains. By increasing the concentration of T2-ORH, the domain of T2-ORH is dominant which act as defect position for the charge transport. Therefore, the optimum morphology is produced from PTB7-Th:T2-ORH:ITIC (1.0:0.5:1.5) photoactive layers leading to the improved charge transport and collection.

**References**

1. T. Lee, Y. Eom, C. E. Song, I. H. Jung, D. Kim, S. K. Lee, W. S. Shin, E. Lim, *Adv. Energy Mater.*, 2019, 0, 1804021.
2. S. Hong, H. Kang, G. Kim, S. Lee, S. Kim, J.-H. Lee, J. Lee, M. Y, J. Kim, H. Back, J.-R. Kim, K. Lee, *Nat. Comm.*, 2015, 2016, **7**, 10279.
3. P. Apilo, M. Välimäki, R. Po, K.-L. Väisänen, H. Richter, M. Ylikunnari, M. Vilkmann, A. Bernardi, G. Corso, H. Hoppe, R. Roesch, R. Meitzner, U. S. Schubert, J. Hast, *Sol. RRL*, 2018, **2**, 1700160.
4. L. Lucera, F. Machui, P. Kubis, H. D. Schmidt, J. Adams, S. Strohm, T. Ahmad, K. Forberich, H.-J. Egelhaaf, C. J. Brabec, *Energy Environ. Sci.*, 2016, **9**, 89-94.
5. T. T. T. Bui, M. Jahandar, C. E. Song, Q. V. Hoang, J.-C. Lee, S. K. Lee, I.-N. Kang, S.-J. Moon, W. S. Shin, *Sol. Energy Mater. Sol. Cells*, 2015, **134**, 148-156.
6. G. P. Kini, S. K. Lee, W. S. Shin, S.-J. Moon, C. E. Song, J.-C. Lee, *J. Mater. Chem. A*, 2016, **4**, 18585-18597.
7. S. Badgujar, G.-Y. Lee, T. Park, C. E. Song, S. Park, S. Oh, W. S. Shin, S.-J. Moon, J.-C. Lee, S. K. Lee, *Adv. Energy Mater.*, 2016, **6**, 1600228.
8. S. Strohm, F. Machui, S. Langner, P. Kubis, N. Gasparini, M. Salvador, I. McCulloch, H.-J. Egelhaaf, C. J. Brabec, *Energy Environ. Sci.*, 2018, **11**, 2225-2234.
9. J. Zhang, Y. Zhao, J. Fang, L. Yuan, B. Xia, G. Wang, Z. Wang, Y. Zhang, W. Ma, W. Yan, W. Su, Z. Wei, *Small*, 2017, **13**, 1700388.
10. T. Zhang, G. Zeng, F. Ye, X. Zhao, X. Yang, *Adv. Energy Mater.*, 2018, **8**, 1801387.